R.I.T

Pumping Potential of a Two-Layer Left-Ventricle-Like Flexible Matrix Composite (FMC) structure

Submitted by,

Arnab Chanda

A Thesis/Dissertation Submitted in Partial Fulfillment of the Requirements for Master of Science in Mechanical Engineering

Department of Mechanical Engineering

Kate Gleason College of Engineering

Approved by:

Dr. Hany Ghoneim	----------
Department of Mechanical Engineering	(Advisor)
Dr. Steven Day	----------
Department of Mechanical Engineering	(Committee Member)
Dr. Alexander Liberson	----------
Department of Mechanical Engineering	(Committee Member)
Dr. Agamemnon Crassidis	----------
Department of Mechanical Engineering	(Department Representative)

Rochester Institute of Technology

Rochester, New York

Feb 7th, 2014

Abstract

The Left Ventricle (LV) can be considered to be a near-conical fibrous Flexible Matrix Composite (FMC) structure in which the myocardial fibers contract by a maximum of 15% in length while pumping to cause an approximately 50% overall volume contraction. The Pumping Potential (PP), defined as the relative volume reduction due to an input stroke, of a simple conical structure was estimated numerically to be approximately 1-2. However, the actual PP of the near-conical LV structure is in the range of 3.3-4. And the question crops up: what is the cause of such a high PP of the LV? To investigate this, the LV is modeled physically and using the finite element software ANSYS. The modeling is based on a recent concept of Helical Ventricular Myocardial Band (HVMB), according to which the heart is made of a single band called the HVMB, which twists and loops to form the heart. Multiple goat hearts are dissected and unfolded into the HVMB. The shape of the band as well as the crude fiber orientation in its outermost (epicardium) and innermost (endocardium) layers are observed. The trace of the band together with the two-layer fiber orientation is recorded, and a Matlab program is written to numerically twist and loop the band into a simple and practical near-conical two-layer LV-like FMC model. Polyurethane (Matrix material) and shape memory alloys (as actuating fibers) are used to physically construct the model. The experimental and analytical investigations yielded a reasonably high PP in the range of 2.5-2.8. Moreover, the twist phenomenon and wall thickening effects, which have been previously pointed out in literature to contribute to the high PP of the LV, were observed clearly in the simulations.

Acknowledgement

I would like to take this opportunity to thank everyone directly and indirectly involved with my research work, for their valuable help and support. I am extremely grateful to my advisor Dr. Ghoneim for giving me the opportunity to work under his guidance. In these two years, I have seen a lot of ups and downs, and there had been days when I felt as if I reached a complete deadlock. I greatly appreciate Dr. Ghoneim for being an endless source of encouragement and motivation through all my good and tough times. The confidence he has shown in my work inspires me to always deliver the best performance.

I would like to thank my thesis committee members Dr. Day, Dr. Liberson and Dr. Crassidis for taking the time to review and evaluate my thesis work. I am also grateful to Mr. Robert Kraynik in the Mechanical Engineering Department's machine shop, for his help with the fabrication of my experimental setup. I am also thankful to Dr. Hensel and all the staff of the mechanical engineering department for their valuable advising during the course of my graduate studies at RIT.

I would like to thank my parents and sister for their support and belief on me throughout my journey in graduate school at RIT. My special thanks to Zhen Yin and all my friends who have always been there for me. I hope my accomplishment today gives all of you a reason to be proud of me.

Arnab Chanda

Table of Contents

List of Figures

List of Tables

Nomenclature

L_o	Initial length
ΔL	Change in length
D_o	Initial diameter
ΔD	Change in diameter
V_o	Initial volume
ΔV	Change in volume
θ	Angle subtended by a band for one conic rotation
Ω	Total band angle

Abbreviations

LV	Left Ventricle
FMC	Flexible Matrix Composite
PP	Pumping Potential
HVMB	Helical Ventricular Myocardial Band
MRI	Magnetic Resonance Imaging
LS	Left Section
RS	Right Section
DS	Descending Section
AS	Ascending Section
IS	Intraventricular Septum
SMA	Shape Memory Alloy
PU	Polyurethane
DOF	Degree of Freedom
PA	Pulmonary Artery
DT	Diffusion Tensor
FE	Finite Element

1. Introduction

The Left Ventricle (LV) is the most essential pumping member of the heart. The LV can be considered to be a near-conical fibrous flexible matrix composite (FMC) structure [8]. An FMC comprises of fibers and a flexible matrix. Moreover, a single layer in a FMC is called a 'lamina' and a stack of laminas is called a 'laminate.' The LV may be assumed to be a multi-layer laminate structure and fall in a special category of 'angle-ply' laminate [10, 11, 12] which shows interesting properties of high Poisson's ratio etc. In order to better understand the LV structure, a basic understanding of the composite materials is important.

In the near-conical LV structure, the myocardial fibers contract by a maximum of 15% to engender an approximate overall 50% volume contraction [1, 2]. The Pumping Potential (PP), defined as "the relative volume reduction due to an input stroke" [11, 12], of a simple conical structure was estimated numerically to be approximately 1-2. However, the actual PP of the LV is in the range of 3.3-4. And the question crops up: what is the cause of such a high PP of the LV? Our current research attempts to investigate the same using crude experimental and analytical modeling of the LV.

In our current research, the heart modeling is based on a recent concept known as Helical Ventricular Myocardial Band (HVMB), according to which the heart is made of a single band called the HVMB, which twists and loops to form the ventricles. Multiple goat hearts are dissected to unravel the HVMB. From literature and dissection results, the HVMB shape and a crude fiber orientation across the top and bottom layers of the HVMB are recorded. A simple

two-layer left-ventricle-like FMC structure is modeled and its PP is investigated experimentally and analytically.

A brief overview of the heart and composite materials is presented in Chapter 1. A comprehensive literature review of the LV structure, the HVMB, our previous work on single-layer FMC LV-like structure, some high PP structures and cardiac modeling techniques are presented in Chapter 2. The key objectives of our research and our preliminary work are discussed in Chapters 3 and 4 respectively. Chapter 5 discusses the experimental and analytical work, followed by the results of the PP of the two-layer LV-like FMC structure in Chapter 6. Chapter 7 presents the conclusions.

1.1 The Heart

The heart pumps out approximately 4.7-5.7 liters of blood in every beat/cycle [3]. The heart is confined in a pericardial sac [3] and is made of three main layers of fibers. The outer most fiber layer is called the 'Epicardium,' the middle (actuating) layer the 'Myocardium' and the inner most layer the 'Endocardium.'

The heart structure comprises of four main parts [3] namely the 'Right ventricle', 'Left ventricle,' 'Right atrium' and 'Left atrium' (Figure 1). Two large veins, namely the 'Superior vena cava' and the 'Inferior vena cava,' carry blood out and into the heart respectively (Figure 1). Two valves, namely the 'Mitral valve' and the 'Tricuspid valve' do not allow the reverse flow of blood from the ventricles to the atriums (Figure 1). Two more valves, namely the 'Pulmonary valve' and 'Aortic valve,' prevent the reverse flow of blood from the arteries to the ventricles.

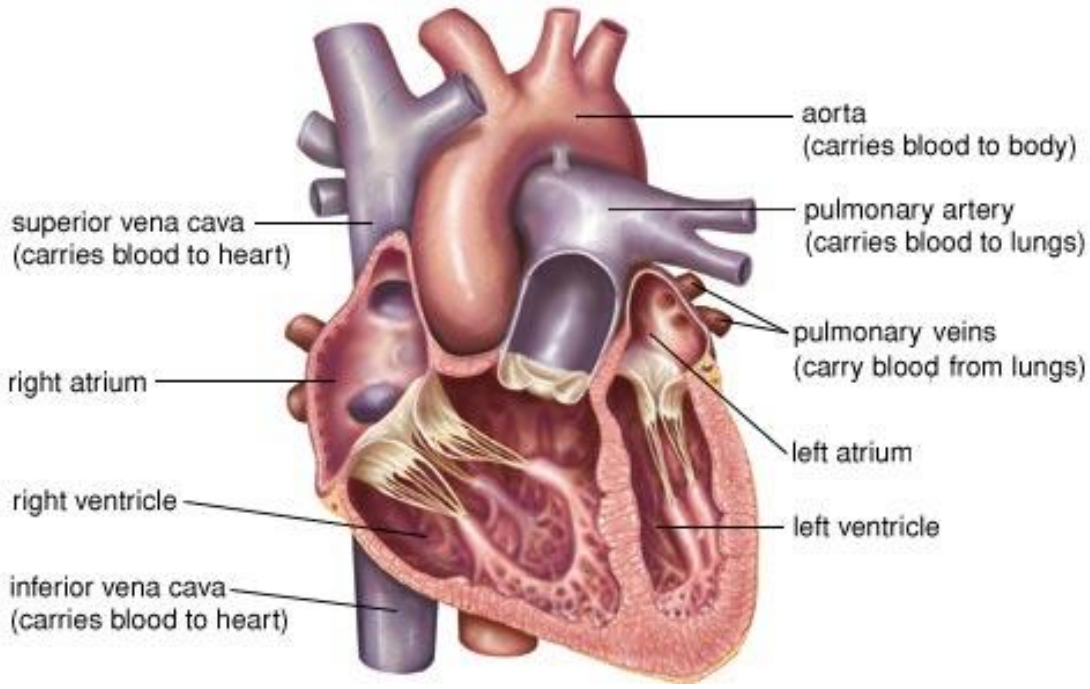

Figure 1: Various components of the human heart [4]

1.2 Composite Materials

A composite material is made by combining two or more materials with distinct physical or chemical properties. Its characteristics are completely different from the individual materials which are combined to make it. In a composite, the individual materials retain their characteristic physical, chemical and mechanical properties. The two constituents of a composite material are 'fibers' and the 'matrix.' Moreover a single layer in a composite is called a 'lamina,' and a stack of laminas is called a 'laminate'.

The fibers are responsible for providing the strength and stiffness to a composite material. The fibers can be broadly classified as continuous (Figure 2(a)) and discontinuous fibers (Figure 2(b)).

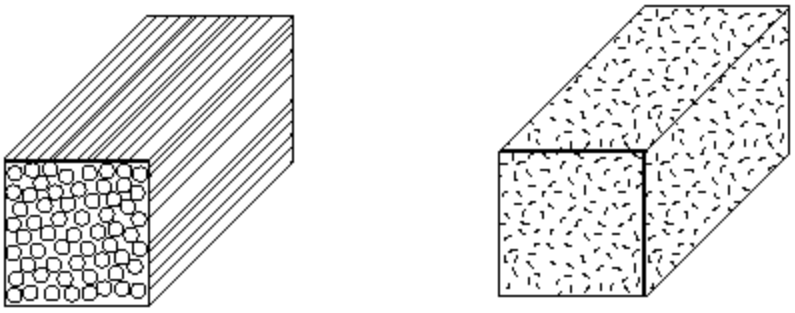

(a) (b)

Figure 2: Fiber classification: (a) Continuous fibers and (b) Discontinuous fibers. Reproduced from [5]

The matrix material in a composite holds the fibers in place and gives a shape to the composite. In a composite under loading, the matrix shares and also transfers the load to the fibers. The matrix can be either a polymer, metal, or ceramic. A polymer has a low strength and stiffness. An 'elastomer/rubber' is a type of polymer with high elasticity, which may stretch more than twice its original length. A common example of elastomer is 'polyurethane (PU).' It has a good tear strength, low water absorption and high biocompatibility [6]. For our current research work, PU has been used as the matrix material for construction of the LV-like Flexible Matrix Composite (FMC) structure.

A single layer of composite material is called 'lamina.' A lamina comprises of a set of fibers placed in a single direction within a matrix material, and is typically orthotropic in nature. In a lamina under loading, the fibers carry the longitudinal and compressive loads, while the matrix distributes the loads among the fibers and also prevents the lamina from buckling under compressive loading. An arrangement of multiple laminas, stacked at different angles, is called a

'laminate.' Figure 3 shows a couple of composite laminas with different fiber orientations stacked together to form a composite laminate structure.

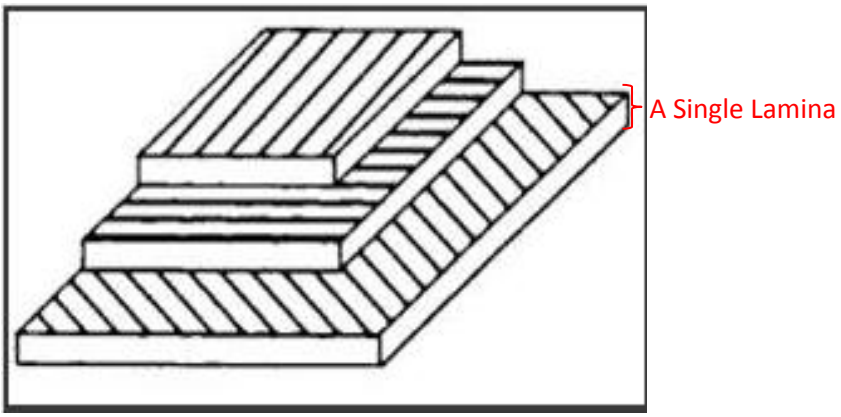

Figure 3: Typical laminate structure: A stack of laminas. Reproduced from [7]

Angle-ply is a special case of laminate in which for every Θ-ply, there is a negative Θ-ply. An example is [Θ_1, Θ_2, $-\Theta_2$, Θ_3, $-\Theta_3$, $-\Theta_1$]. Furthermore angle-ply laminates can be of two types namely 'symmetric angle-ply' and 'asymmetric angle-ply.' In a symmetric angle-ply laminate, the laminas are arranged as mirror image from middle surface. An example is: [Θ_1, Θ_2, Θ_3, Θ_3, Θ_2, Θ_1] as shown in Figure 4. In an asymmetric angle-ply laminate, the laminas are arranged as negative mirror image from the middle surface. An example is: [Θ_1, Θ_2, Θ_3, $-\Theta_3$, $-\Theta_2$, $-\Theta_1$] as shown in Figure 5.

In our current research, the LV structure has been assumed to be an asymmetric angle-ply laminate with two or three fiber layers everywhere. These fiber layers will be revisited later in the upcoming sections.

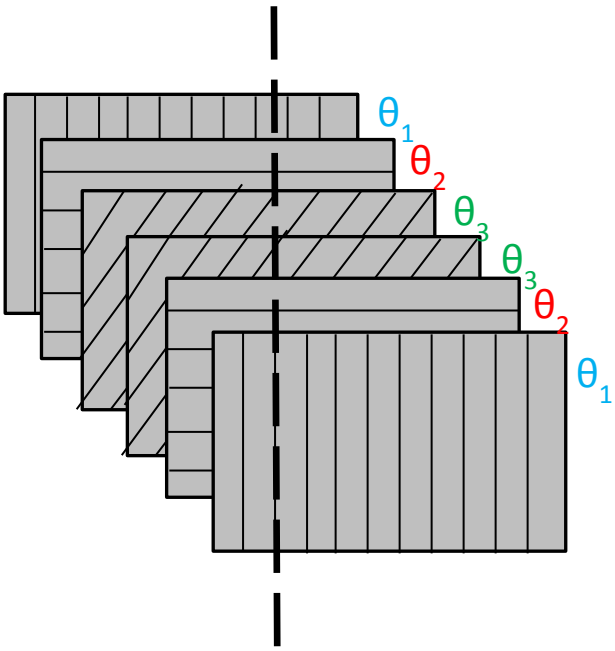

Figure 4: Symmetric Angle-Ply Laminate.

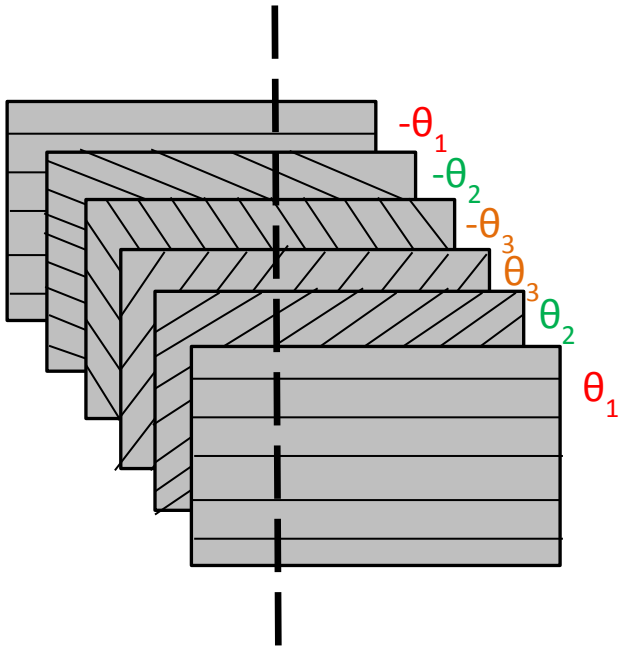

Figure 5: Asymmetric Angle-Ply Laminate.

2. Literature Review

The Left Ventricle (LV) is the most essential part of the heart. The LV structure can be considered to be a Flexible Matrix Composite (FMC) structure [8] with embedded myocardial fibers, arranged in an overlapping helical fashion. Numerous dissection and histological techniques have been employed in the past to explain the LV anatomy. One of the most successful attempts of unraveling the LV anatomy was by Torrent Guasp, a Spanish scientist who spent almost his entire life in this painstaking research on dissecting the heart. He proposed that the heart is made of a single band known as the Helical Ventricular Myocardial Band (HVMB), which twists and loops to form the heart.

Recent advancement in imaging techniques has enabled researchers to study the heart in detail, and also model it. Cardiac modeling has been used so far mainly to study heart anatomy,

pumping mechanisms, and also to model diseased hearts. However, minimal effort has gone into the study of the effect of fiber orientation of the heart on its pumping action. Recently, the fiber orientation of the HVMB was studied by Ghoneim and Arnab [9], and a LV-like FMC structure was modeled using the simplest crude fiber orientation observed in the HVMB endocardium. The Pumping Potential (PP) of the simple single-layer-LV-like FMC structure was investigated both experimentally and analytically. The experimental and analytical PP observed were 1.67 and 1.9 respectively. Though a reasonably high number, the resulting PP is much lower than that of the human heart, which is approximately 3.3-4 [1, 2]. Previously, Ghoneim, based on an idea proposed by Lawrie [10], that an asymmetric angle-ply FMC structure can produce pumping with a very high PP, investigated two asymmetric angle-ply FMC structures [11, 12], which yielded high PP values. The LV structure can be assumed to be an asymmetric angle-ply FMC structure. In our current research, the effect of the simplest, practical and most accurate fiber orientation in the two predominant layers, namely the epicardium (topmost) and the endocardium (bottommost) of the LV, on its PP is investigated both experimentally and analytically.

A comprehensive overview of the LV structure is presented in Section 2.1 and the recent Helical Ventricular Myocardial Band (HVMB) concept is presented in Section 2.2. Some angle-ply FMC structures with high PP, investigated by Ghoneim et al. are presented in Section 2.3. Our preliminary work on the single-layer LV-like FMC structure has been discussed in Section 2.4. Section 2.5 presents a brief but up-to-date literature on the cardiac modeling.

2.1 Left Ventricle (LV) Structure

The LV structure was a mystery for a long time. In 1628, Harvey for the first time pointed out to the possible functional significance of the myocardial (actuating muscular layer which causes pumping action in heart) fiber orientation in the LV [13]. Stensen, 1664 [15], Lower, 1669 [16], Senec, 1749 [17], MacCallumetal [19] and Mall, 1911 [20] found that the LV structure can be considered to be made of three main fiber layers, in which the inner and outer fibers are helical and the middle layer is mainly circumferential. Ludwig [18], later in the nineteenth century, observed the LV can be considered to be an approximate asymmetric angle-ply structure, with the epicardial (outermost layer) fibers crossing the endocardial (innermost layer) fibers at approximately right angles.

In 1961, Streeter et al. [21] dissected a dog's heart and reported the various myocardial fiber orientations observed going from the endocardium to the epicardium. In Figure 6, the three-dimensional segment of the LV wall illustrates mean myocardial fiber orientation. The apex-base direction is vertical, and the horizontal edges of the block are parallel to the circumferential plane, as shown in the Figure 6. Streeter et al. [21] observed that the LV myocardial fibers halfway between the endocardium and epicardium are circumferential, at a fiber angle of 0° (Figure 6, 7). The fibers at the endocardial and epicardial surface were found to overlap at a 120° angle and form opposite 60° angles with circumferential myocardial fibers. Also, the fiber angles were observed to vary gradually between these extremes. Figure 7 presents a plot showing the relation observed by Streeter et al. [21] between the LV wall thickness and the myocardial fiber angle distribution going from the endocardium (minimum wall thickness) to the epicardium

(maximum wall thickness), during systole and diastole respectively. The fiber angle distributions, as can be observed in Figure 7, change minimally from systole to diastole.

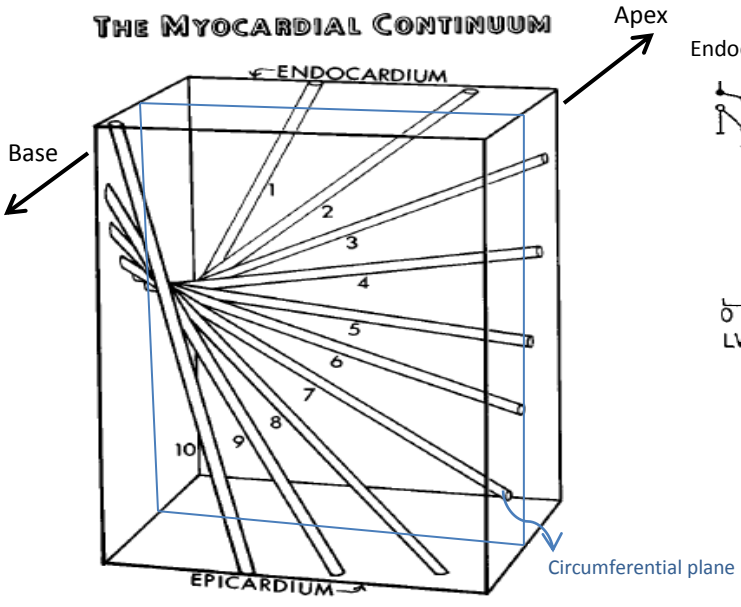

Figure 6: 3-Dimensional section of dog's LV wall myocardium showing the 10 layer fiber arrangement [21]

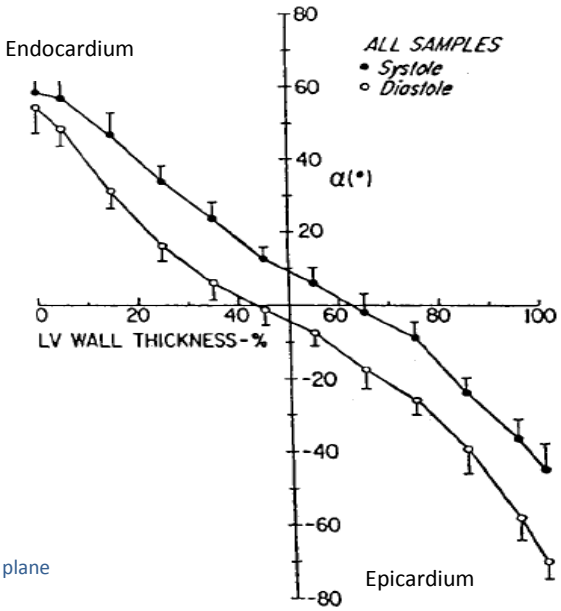

Figure 7: LV wall thickness versus fiber angle distribution [21]

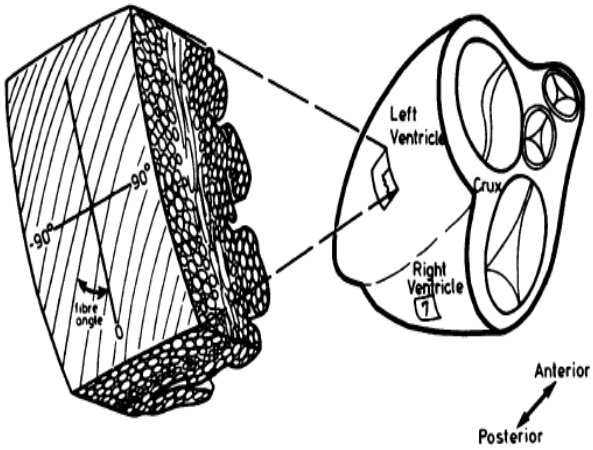

Figure 8: Orientation employed for block removed from serial section, in Histology [22]

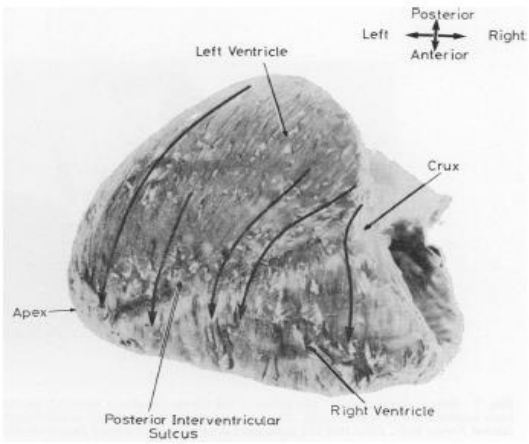

Figure 9: Fiber orientation at the crux and apex of a left ventricle wall [22]

In 1981, Greenbaum et al. [22] studied the fiber orientation in the LV of the human heart, via dissection and histology (Study of cells and tissue structures at a microscopic level). He observed that the LV structure is an approximate asymmetric angle-ply structure (Figure 8). He also pointed out the approximate fiber orientations near the base, apex and in the middle, on the septal side of the LV (Figure 9).

Until the late 1980's, the LV was considered to be made of a homogeneous material, and all the myocardial fibers were assumed to contract together simultaneously, while the heart (or the LV) pumps. These facts were used in modeling of the LV, and were supported by various two-dimensional imaging techniques, such as echocardiography and angiography. However recently, Diffusion Tensor Magnetic Resonance Imaging (DT-MRI) [24] and Echocardiography have enabled researchers to understand the highly anisotropic structure of the LV, the multi-step myocardial contraction/activation schemes, ventricular twisting [23], and many other important phenomena in the heart. These findings have significantly helped to improve the cardiac modeling techniques.

Recently, the Helical Ventricular Myocardial Band (HVMB) model [14] has defined a new approach towards an understanding of heart anatomy. According to the model, the heart is made of a single band of muscle fibers, which twists and loops to form the two ventricles. This novel concept has been used as the modeling hypothesis in our current research. The HVMB model is discussed in detail in Section 2.2.

The University of Auckland group [8] studied the LV at the microscopic level and proposed that the LV structure can be considered to be made of a fibrous Flexible Matrix Composite (FMC) material, with myocardial fibers arranged in different laminas/sheets, separated by a collagen matrix material (Figure 10).

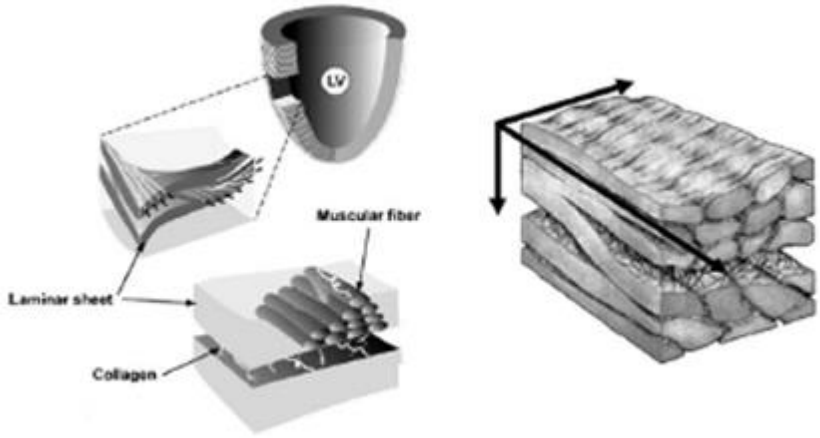

Figure 10: University of Auckland 'laminar sheet' model [8]

2.2 Helical Ventricular Myocardial Band (HVMB)

Dr. Torrent-Guasp in 2005 [14] proposed the Helical Ventricular Myocardial Band (HVMB) concept, as a result of his 25 years of research, aimed at the dissection of the heart into a single fibrous band, which can twist and loop to form the heart. The credibility of his research lies in the dissection of more than a thousand hearts of different species (including mammalian hearts, human hearts, fish hearts and reptile hearts) [25]. The major dissection steps followed by Dr. Torrent-Guasp are shown in Figure 11. The more detailed dissection steps are discussed in Figure 12.

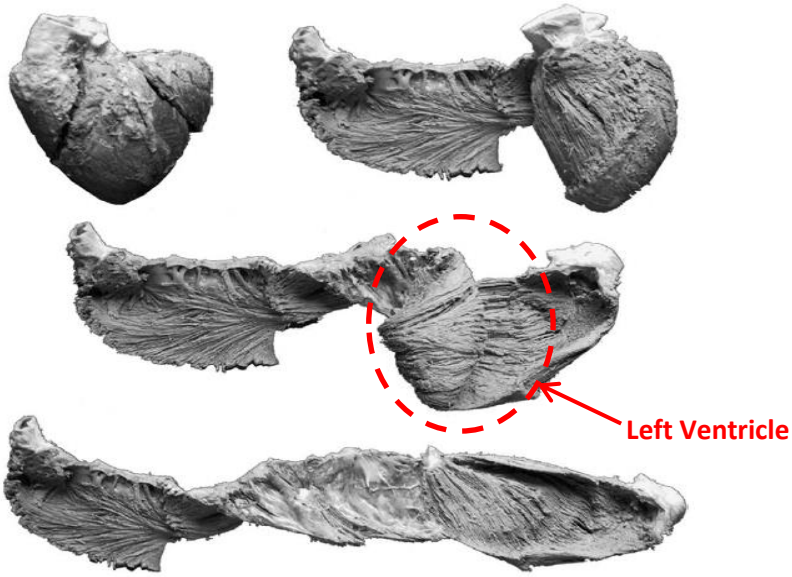

Figure 11: Major dissection steps: The Helical Ventricular Myocardial Band (HVMB) [14]

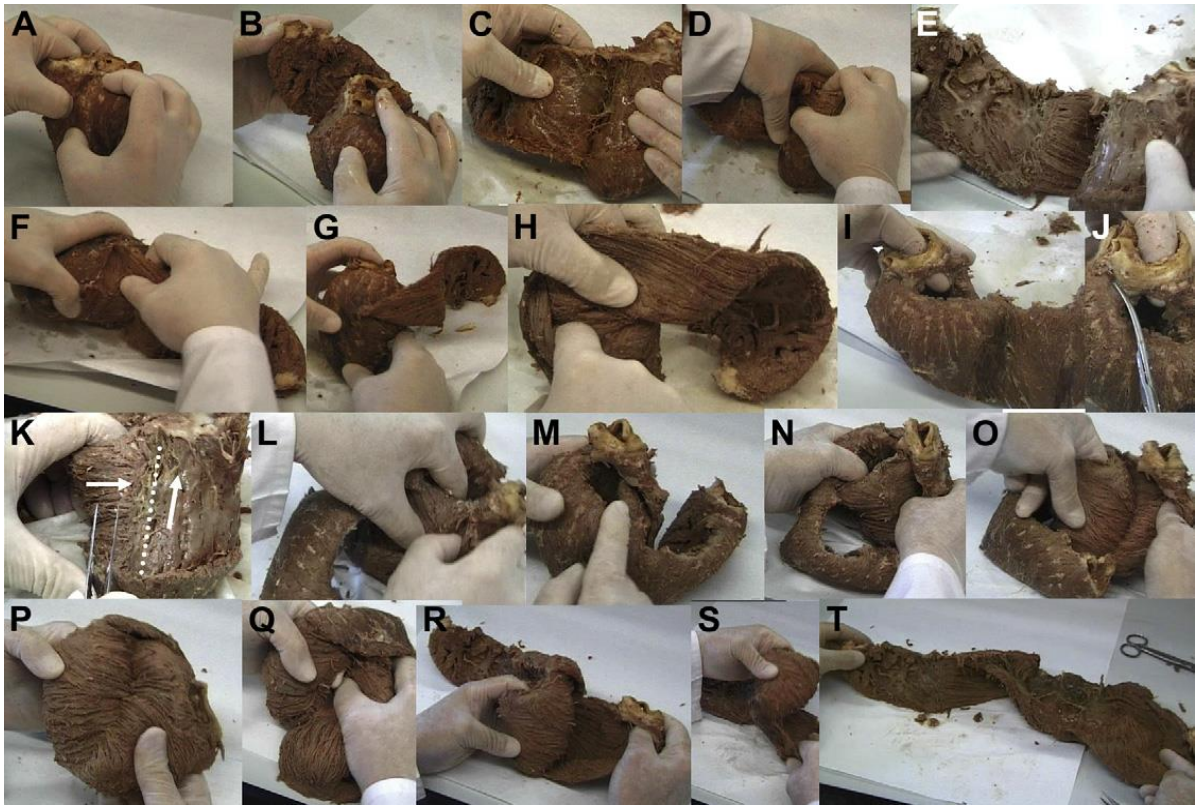

Figure 12: Detailed HVMB dissection steps [14]

The first step before dissection is to boil the heart in water for about an hour to loosen the connective tissues [14]. The next step is to remove all the unnecessary fat from the epicardial (outer) surface. The pulmonary artery and aorta are separated (Figure 12 A). At the anterior interventricular sulcus (Figure 12 A, magnified image in Figure 13 A), some bridging superficial fibers (also called aberrant fibers) are cut through, and the right ventricular (RV) free wall is moved aside (Figure 12 B). The ending edge of the RV free wall is called the 'Posterior interventricular sulcus.' To move further in dissection, the RV free wall is pushed laterally, followed by cutting through fibrous trigons. In this way, the basal loop is unfolded (Figure 12 E).

Looking from the RV side, the apical loop comprises of two clearly distinguishable fiber layers (Figure 13 B), namely a deeper layer (descendent section (DS)) and a more superficial layer (ascendant section (AS)). These fiber layers cross each other at approximately right-angles forming the septum (a thin membrane which separates the LV and RV cavities) as shown in Figures 12 (K), 13 (B) and 14. To continue with dissection, the posterior interventricular sulcus is revisited. The aorta is separated from the LV by cutting though the fibrous trigons attaching them. The separated AS (ending at the aorta) is un-looped all the way followed by the unlooping of the DS, to unravel the full HVMB. The flat un-looped HVMB is shown in Figure 15.

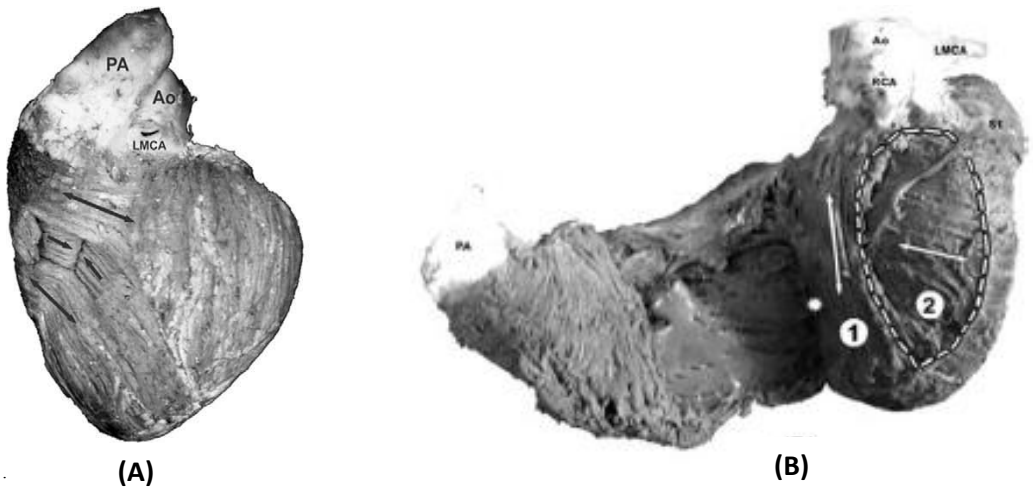

Figure 13: (A) Anterior interventricular sulcus (AIS): Double headed arrows show the bridging aberrant fibers. Single headed arrows show the two actual fiber directions separated by the AIS. (B) Interventricular septum with the ascendant fibers (AS, 1) fibers crossing the descendant fibers (DS, 2) at right angles, observed from the RV side. Reproduced from [14]

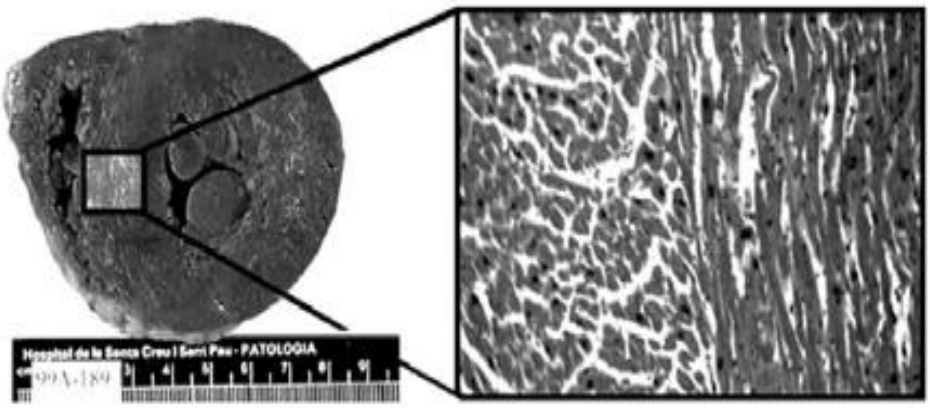

Figure 14: Microscopic view of the top of septum, showing the two distinct fiber groups, namely AS and DS. Reproduced from [14]

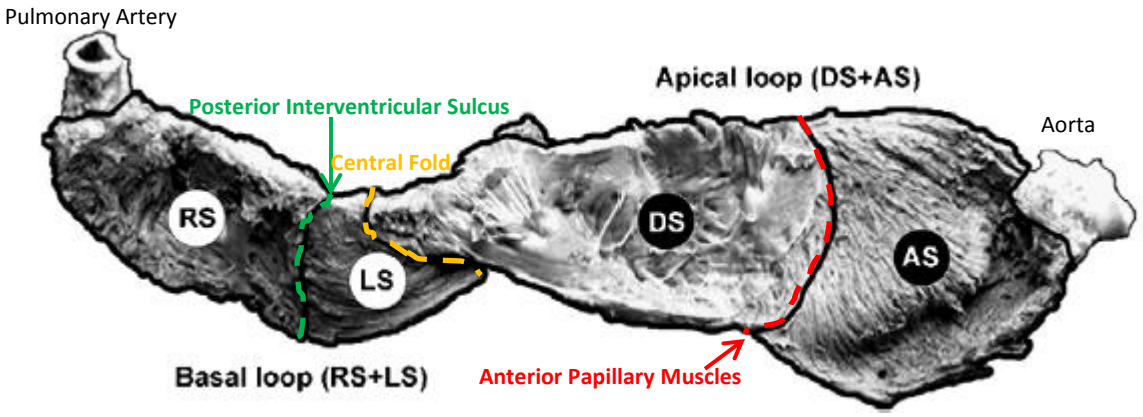

Figure 15: Different sections of the flat HVMB band. [14]

The HVMB is divided in two main sections, namely the basal loop (from pulmonary artery to central 180^{o} fold) and the apical loop (from central 180^{o} fold to the aorta) [14] (Figure 15). Both of these loops are further subdivided into two sections respectively (Figure 15). The basal loop is divided into the Right Section (RS) and the Left section (LS), separated by the posterior interventricular sulcus. The apical loop is divided in the descending section (DS) and the ascending section (AS), separated by the anterior papillary muscle.

The RS in the HVMB forms the RV and the LS, DS and AS together forms the LV. Moreover, the HVMB twists and loops one half turn to form the RV and a one-and a-half turn more to form the LV.

HVMB dissection has been recently performed to study the interventricular septum (IS) structure [14]. It has been found that the IS belongs to both the Left and the Right ventricles. The IS comprises of AS and DS fibers from the LV side and recurrent fibers from the RV side. Figure 16 (A) shows the various fiber groups (i.e. AS, DS etc.) forming the LV, RV and IS respectively.

Figure 16 (B) emphasizes the three major fiber groups participating in the IS formation. These three layers have also been recorded through our dissection of goat hearts.

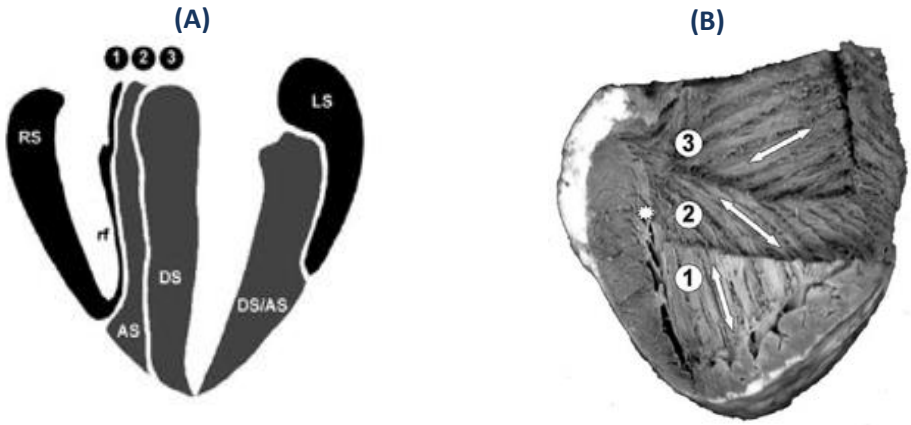

Figure 16: (A) The various fiber groups forming the heart structure at different regions. (B) Three main fiber layers forming the interventricular septum. [14]

2.3 High Pumping Potential Structures

Lawrie et al. [10] proposed a novel idea that an asymmetric angle-ply FMC structure can be used to produce pumping with a very high PP. Based on this idea, the PP of a cylindrical pump by Lawrie [10] and a novel actuator by Shan et al. [26] were investigated. Ghoneim et al. extended Lawrie's work to investigate two asymmetric angle-ply FMC structures under axial loading, namely a barrel shaped [11] and hyperbolic [12] structure. The schematic of these two FMC structures, investigated by Ghoneim et al. are shown in Figure 17 (A, B). In both of these structures, carbon fibers were wound in two layers, wetted by polyurethane resin (Adiprene KX208, from ChemPoint), to form a $[\pm\theta_f]$ angle-ply FMC laminate. The snapshots of these two structures are shown in Figure 18 (A, B). The PP of these structures is listed in Table 1.

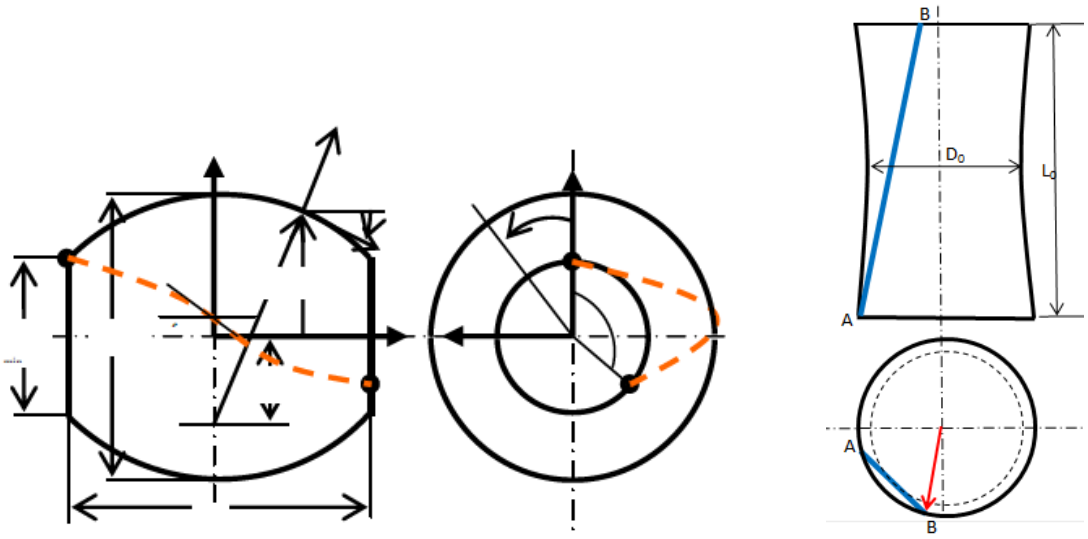

(A) (B)

Figure 17: Schematic of the asymmetric angle-ply FMC structures investigated by Ghoneim et al. (A) Barrel-shaped [11] and (B) Hyperbolic [12]

(A) (B)

Figure 18: Snapshots of asymmetric angle-ply FMC structures investigated by Ghoneim et al. (A) Barrel-shaped [11] and (B) Hyperbolic [12]

Another idea was also investigated by Ghoneim [27], which is based on torsional loading of a hyperbolic single-ply FMC structure. The schematic of the hyperbolic single-ply FMC structure, with rigid fibers and very low matrix stiffness, is presented in Figure 19. Upon twisting the structure by an angle,Φ, the length decreased from L_0 to L_1 and the throat diameter decreased from D_0 to D_1 respectively thus producing a reasonable volume contraction (pumping action).

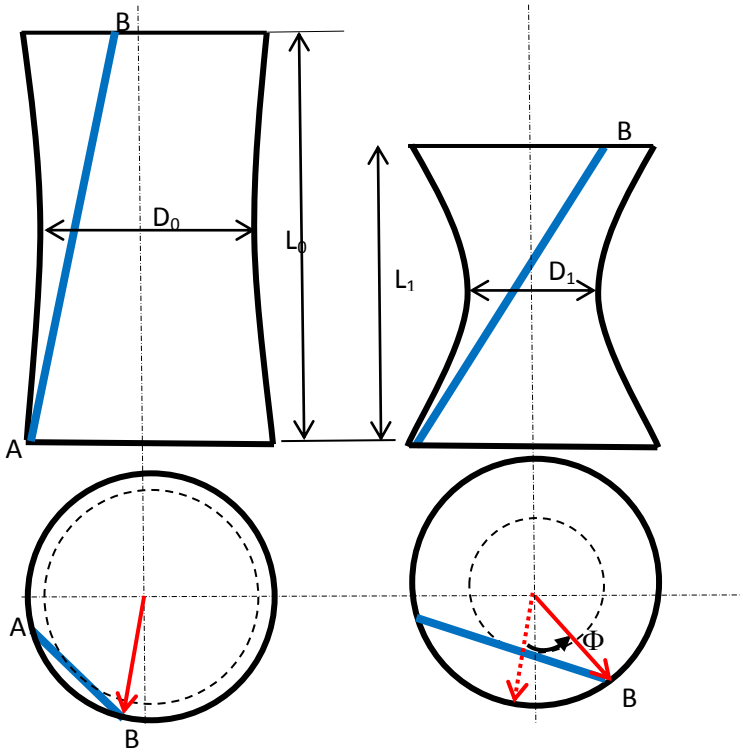

Figure 19: Schematic of volume reduction (pumping action) in a single-ply hyperbolical FMC structure upon twisting [27]

The PP of the different pumping structures, in the literature, is displayed in Table 1. Though the PP of the simple single-layer near-conical LV-like structure (discussed in Section 2.4) is relatively high compared to the cylinder-piston classical pumping structure, it is still well below that of the heart.

Structure	PP
Cylinder-Piston	1.00
Single-layer LV-like FMC structure	1.67 -1.88
Hyperbolic	2.59
Heart [1, 2]	3.3- 4.0
Barrel Shaped	10.33

Table 1: Pumping Potential of FMC structures

2.4 Single-Layer-Left-Ventricle-Like FMC Structure

A near-conical single-layer LV-like FMC structure [9] was modeled, and investigated experimentally and analytically (using finite element software ANSYS). The modeling was based on the HVMB concept discussed in Section 2.2. Multiple goat hearts were dissected and unfolded into the HVMB. The shape of the band was observed. An idealized fiber orientation was assumed to run along the longitudinal axis of the band (principal fiber direction). The trace of the relevant portion of the band comprising the LV and the assumed fiber orientation was recorded, and a Matlab program was written to numerically twist and loop the band into a near-conical LV-like structure (Figure 20).

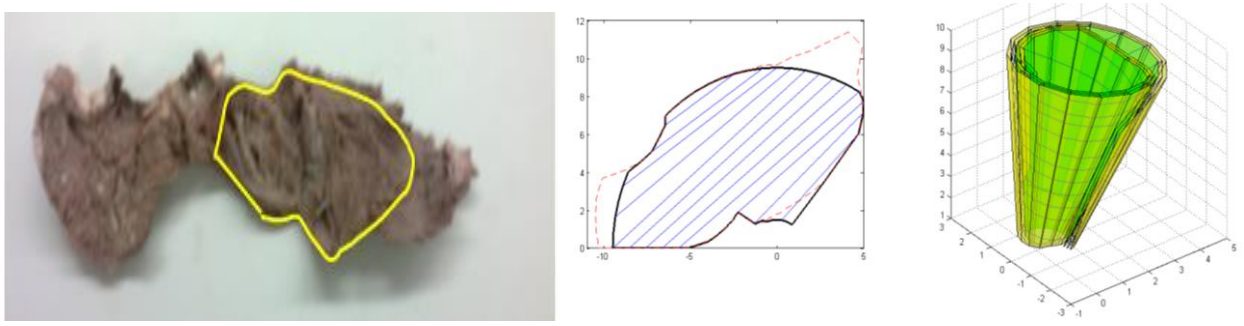

(A) (B) (C)

Figure 20: (A) Part of the HVMB band constituing the LV structure. (B) The LV band and crude single-layer fiber orientation plotted in Matlab. (C) Rolled near-conical LV-like structure with rolled fibers, plotted in Matlab. [9]

A closer look at the generated near-conical LV-like structure is presented in Figure 21. It is noticed that there are two unique sides of the structure:

1. A descending/ascending side, which is made of two overlapped layers. The fiber orientations of the two layers are different. The two layers constitute an angle-ply laminate.
2. An ascending side, which is constituted of a single layer and has a predominantly circumferential fiber orientation.

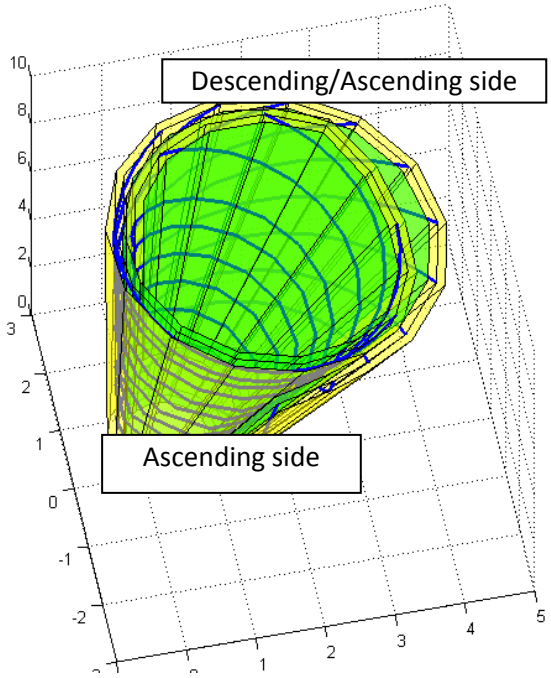

Figure 21: A closer look at the near-conical LV-like structure

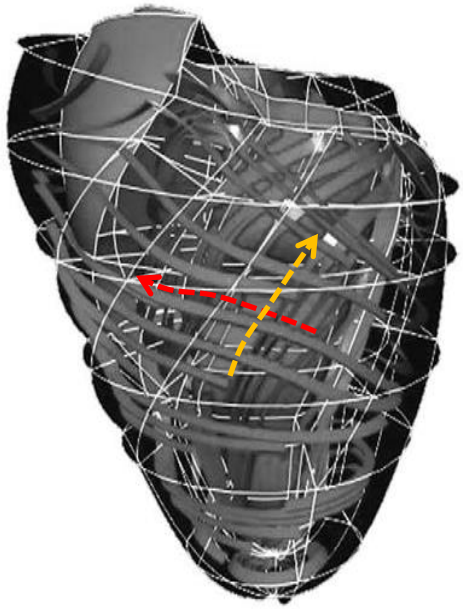

Figure 22: Laminar structure of the heart [14]

It should be pointed out that, despite the idealized fiber orientation adopted (Figure 21), the engendered 3D fiber orientation (Figure 22) captures some of the main features of the heart's LV muscle fibers orientation. The two clear ones are [14]:

1. Two crossed fiber populations exist in one portion of the ventricle wall as shown in Figure 22 (descending/ascending).
2. The populations of the fibers consist of a continuous and helical structure.

These structural observations significantly affect the pumping action of the LV-like structure, which has been emphasised previously in Section 2.3, discussing high PP structures.

For the experimental investigation, FMC was used to model the heart muscle. Polyurethane (PU) was employed for the matrix and shape memory alloy (SMA) fibers were used as actuating muscle fibers. The LV-like prototype was produced in three steps: (Figure 24 (a, b))

1. The band was produced using the open mold method, where SMA fibers were placed according to the idealized fiber orientation of the goat's heart (Figure 23 A).

2. The band was twisted and looped to form the conical LV-like FMC structure.

3. The base of the conical structure was immersed into a bath of polyurethane to form a polyurethane base (Figure 23 B).

Figure 23 (A): The idealized PU/SMA flexible-matrix composite band [9]

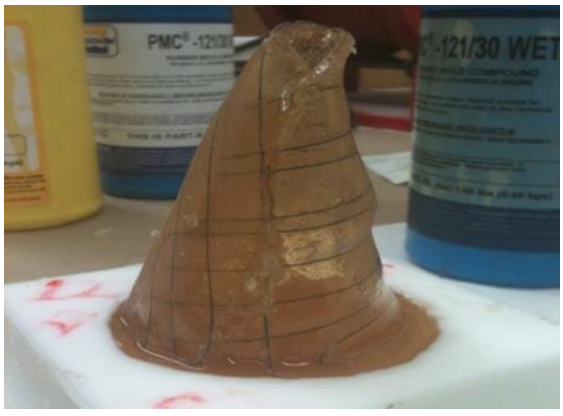

Figure 23 (B): The final conical LV-like structure [9]

The SMA fibers of the prototype model of the LV-like structure were connected to a power supply, and the apex of the conical structure was shoved with a tube extended out from the apex, as shown in Figure 25. The structure was filled with water, and the SMA fibers were charged. As the fibers were activated and heated up, the structure was partially collapsed, pumping out water along the extended tube.

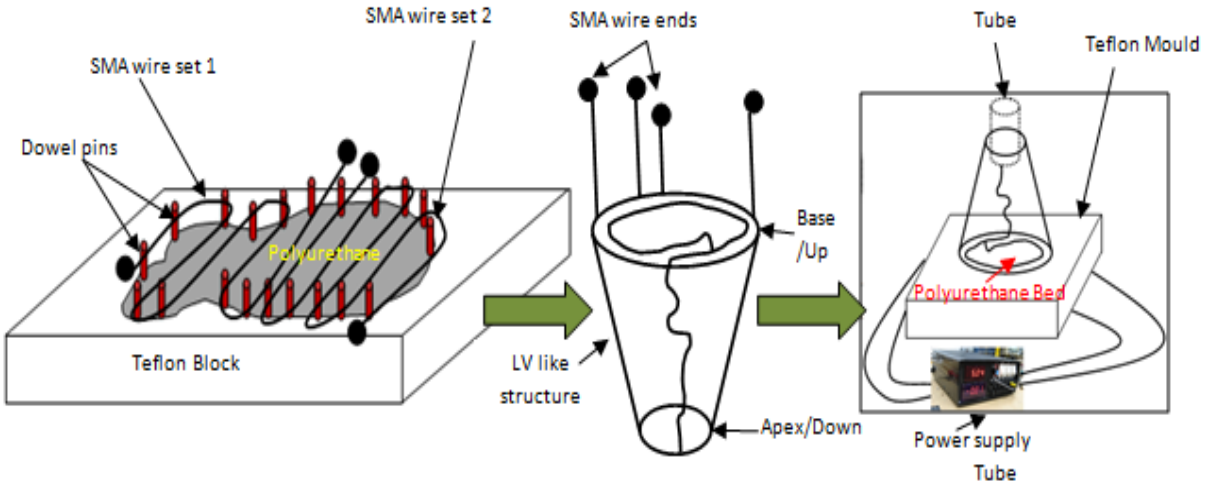

(a) (b) (c)

Figure 24: Figure showing the two phase construction of the LV like structure followed by the experimental setup (c). (a) PU/SMA band in a Teflon mold cut in shape of LV band (b) Rolled PU/SMA band

To estimate the PP of the near-conical LV-like FMC structure, the SMA was charged with the maximum amount of power allowed, which generates the highest strain ($\Delta L//L_0$) in the SMA without destroying the shape memory of the wires. The volume of the displaced water (ΔV) in the extended tube was measured, and the PP of the LV-like FMC structure was computed. The results are presented in Table 2.

Parameter	Experimental	ANSYS
ΔV	2.5 cm^3	3.55 cm^3
V_0	50 cm^3	37.73 cm^3
$\Delta L/L_0$	3%	5%
PP	1.67	1.88

Table 2: Pumping potential of single-layer LV-like FMC structure

Figure 25: The experimental set-up

The analytical investigation was conducted using ANSYS software. The finite element mesh is displayed in Figure 26. The PU matrix was modeled with Solid 186, and the fibers were modeled with Beam 189 elements. The base was held fixed in all DOF and the model was excited with a 5% thermal strain along the fibers. The material properties used in the analysis are given in Table 3. Large deformation analysis was invoked. The experimental and analytical investigation yielded a PP of 1.67 and 1.9 respectively.

Material	Property	Value	Unit
SMA	Modulus of Elasticity	133	GPA
	Poisson's ratio	0.33	
PU	Modulus of Elasticity	20	MPA
	Poisson's ratio	0.48	
Core	Modulus of Elasticity	1	KPA
	Poisson's ratio	0	

Table 3: Material properties of SMA, PU and core material

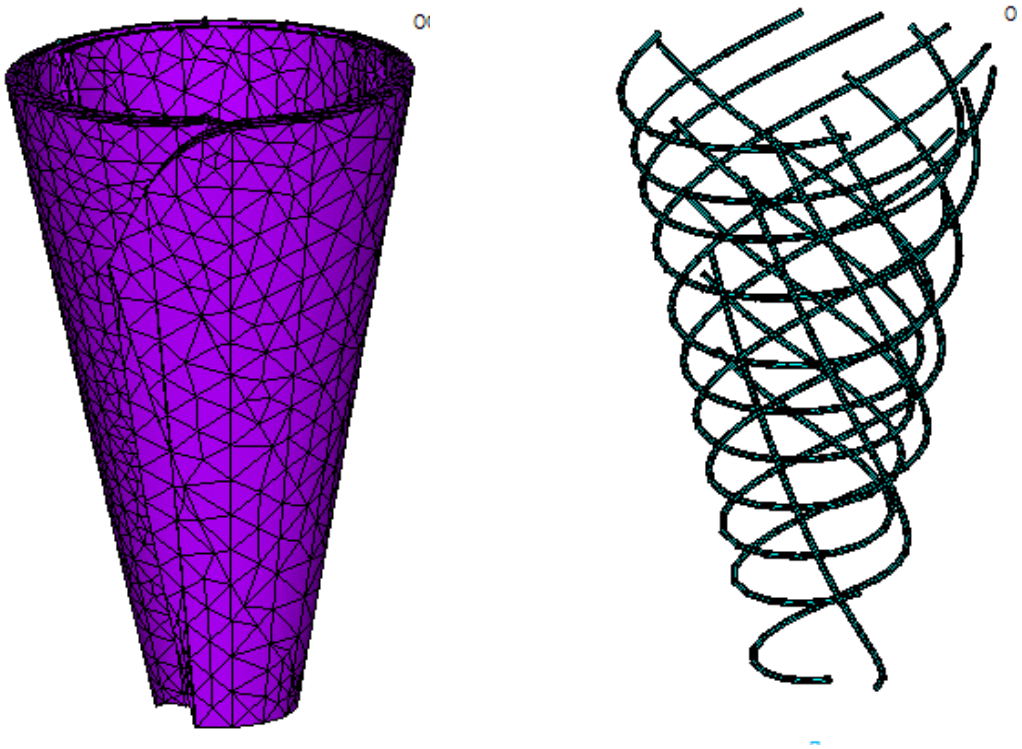

Figure 26: The finite element mesh of the PU matrix (left) and SMA fibers (right). [9]

2.5 Cardiac Modeling

Cardiac modeling helps in understanding the function of the heart, disease propagation in the heart and also cardiac treatment. Typically, Diffusion Magnetic Resonance imaging (DT-MRI) technique or other suitable imaging techniques are used to obtain three-dimensional live images of the heart structure, fibers and different heart components like the ventricles. Subsequently,

these images are converted to appropriate numerical models through various volume and curve fitting post-processing techniques.

The Auckland Bioengineering group in 1991, for the first time, developed a 3D finite element model [28] of the ventricular geometry (Figure 27) and the associated muscle fiber orientation. The geometry and fiber orientation information was obtained through two-dimensional imaging of a beating canine heart. The fiber orientation observed in the epicardium (Figure 28 A) and endocardium (Figure 28 B) formed an approximate asymmetric angle-ply orientation [28].

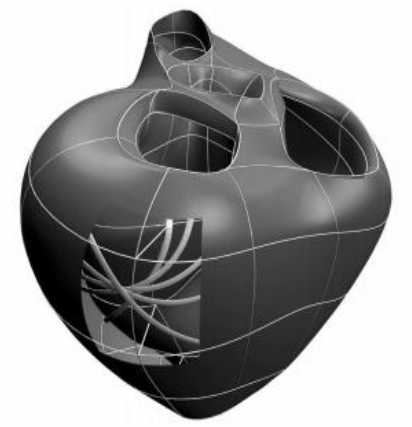

Figure 27: Auckland heart model Geometry Reproduced from [8]

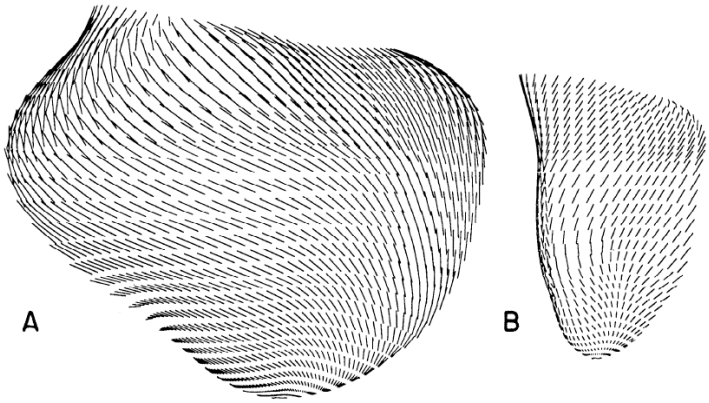

Figure 28: Auckland heart model fiber orientation in Epicardium (A) and Endocardium (B) [28]

Dorri et al. [29] in 2004 designed a finite element model to simulate LV pumping and to study the effect of localized tissue/fiber deaths. The first step followed was to define the geometry of the human heart (Figure 29 A). The epicardial and endocardial surfaces were constructed from the various key points obtained from a human post mortem heart. To obtain the fiber points, a method called SPOT (Fiber Strand Peel-Off Technique) was employed. The fiber points for each

fiber were connected using splines (Figure 29 B). FMC was used to model the LV (Figure 29 C). Figure 29 (D) shows the post-processing result of LV deformation due to systole.

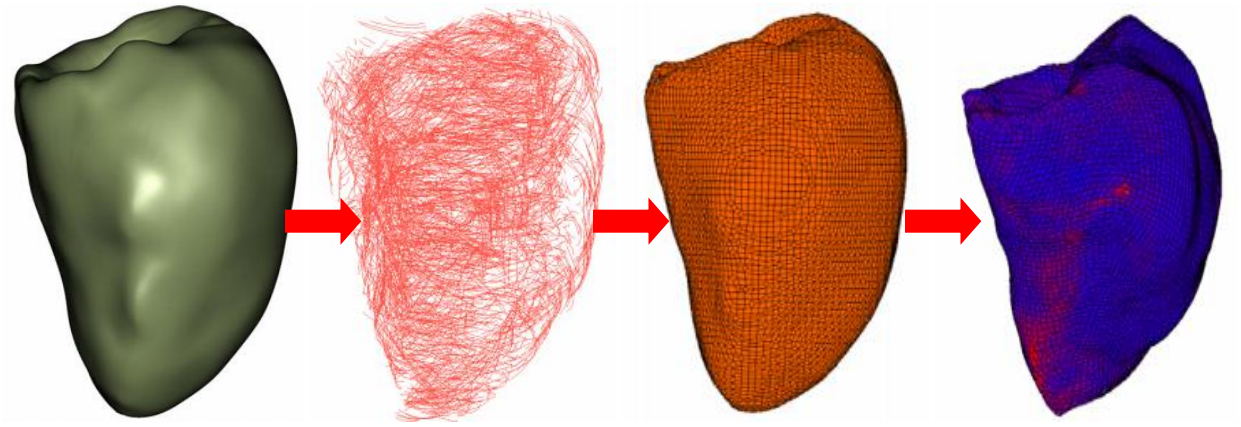

(A) (B) (C) (D)

Figure 29: (A) Heart geometry. (B) Fiber spline plotting. (C) Meshing (D) Systole deformation simulation. Reproduced from [29]

In 2006, Sermesant [30] designed an electromechanical finite element model to simulate the heart functioning. The geometrical modeling and fiber distribution (Figure 30 A, B) were based on interpolation data from USCD [31] and DT-MRI imaging. Moreover, three major fiber groups were identified as shown in Figure 30 (A, B). The blue and red colors represent the fibers crossing at opposite angles (+/- θ) and the yellow color represents the horizontal (circumferential) fibers.

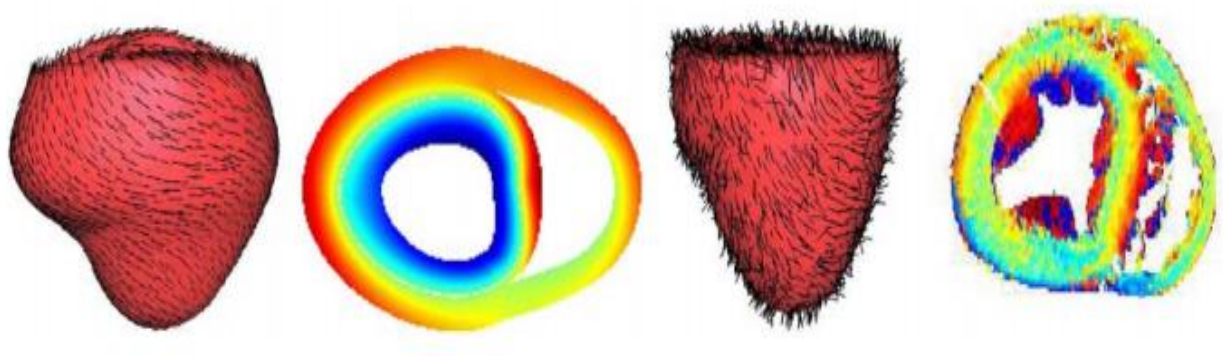

(A) (B)

Figure 30: (A) Fiber orientation from USCD [31]. (B) Fiber Orientation from DT-MRI

In 2008, Wang et al [32] conducted a multi-scale analysis of the cardiac structure. DT-MRI imaging of a rat's heart was used to obtain the heart geometry and fiber orientation. The approximate relative fiber angles of the endocardial, myocardial (Mid) and epicardial layers were identified in the rat's heart DT-MRI images, which are presented in different colors in Figure 31.

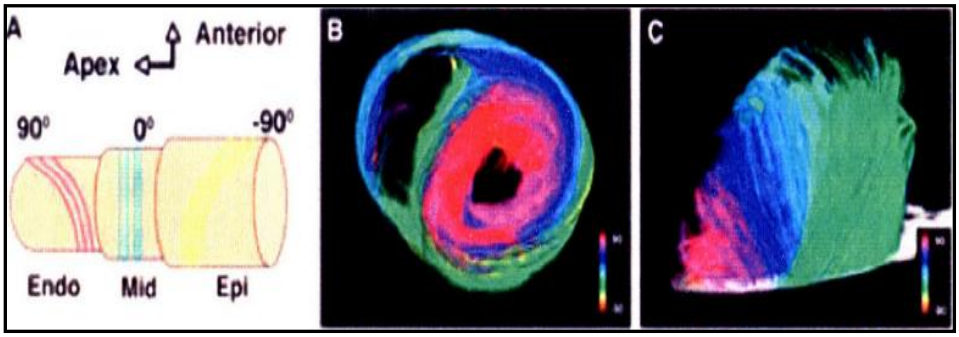

Figure 31: DT-MRI images of a rat's heart and the three main fiber orientations [32]

In 2011, Goktepe et al. [33] designed a finite element (FE) based biventricular heart model (Figure 32). The material properties were based on experimental data from 6 pig hearts [35] and

the myocardial fiber distribution was similar to that in a human heart, obtained using DT-MRI imaging.

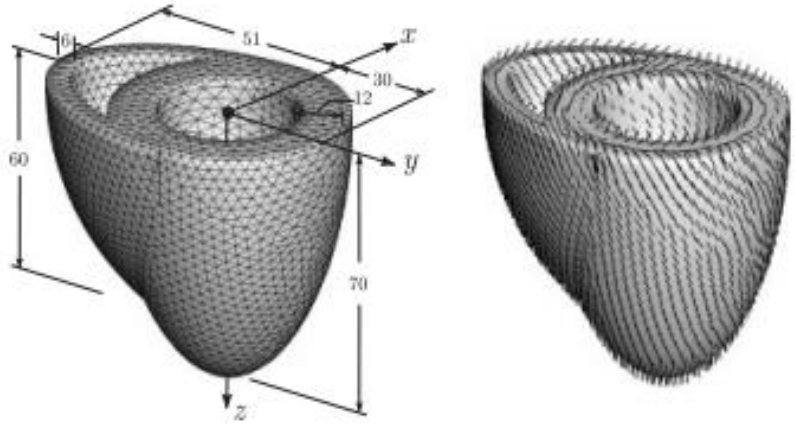

Figure 32: FE biventricular heart model by Goktepe et al [31]

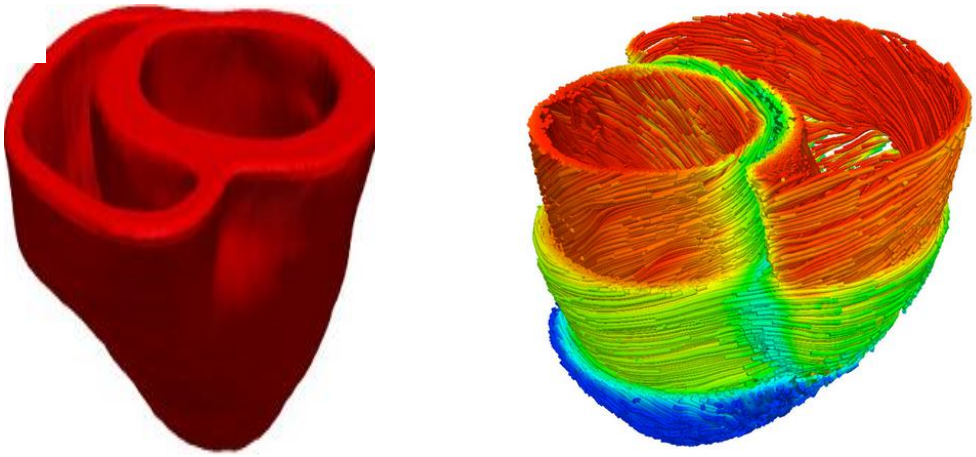

(A) (B)

Figure 33: John Hopkins University canine FE model [36]. (A) Model geometry (B) Fiber structure

Recently in 2012, the computational cardiology lab at John Hopkins University developed a canine heart FE model (Figure 33) [36] to investigate the various mechanisms of heart disease.

DT-MRI imaging was used to construct the geometry and fibers. Moreover, the fibers were categorized into three main groups, namely the circumferential middle layer and vertical outer and inner layers with opposite angles [+/-θ], as shown in Figure 33 (B).

In our current research, the LV has been modeled based on the HVMB hypothesis discussed previously in Section 2.2. The geometry and two-layer fiber orientation adopted is simple, practical (with our current facilities) and supported by literature and dissection results. Moreover, unlike the various cardiac models in literature with a huge number of fibers, the number of fibers considered in our model is very small, to ensure simplicity and practicality of modeling.

2.6 Summary

The LV structure can be considered to be made of a Flexible Matrix Composite (FMC) material [8], with myocardial fibers embedded in a helically overlapping fashion [15, 16], in approximately three distinguishable layers, identified through dissection and histological techniques [17, 18, 21] (Figure 7) and via various imaging techniques [28, 30, 31, 32, 36] (Figures 30, 31 and 33). The inner (endocardium) and outer (epicardium) layers cross each other at opposite angles (+θ/- θ), and the middle layer is mainly circumferential [14, 21, 22, 28, 30, 31, 32, 36] (Figures 7, 8, 16, 28, 31, 33), forming an approximate asymmetric angle-ply laminate structure.

The fiber orientation significantly affects the Pumping Potential (PP) of angle-ply flexible matrix composite structures [10, 11, 12, 26, 27]. The LV (or the heart), which is a natural pump in our body, shows a PP of 3.3-4. In an attempt to shed some light on the effect of fiber orientation of

the LV on its PP, a simple and practical single-layer near-conical LV-like structure was modeled, and its PP was investigated experimentally and analytically. The modeling was based on the HVMB hypothesis, which states that the heart is made of a single band, which twists and loops to form the two ventricles. The single-layer near-conical LV-like structure yielded a PP of 1.67 experimentally and 1.9 analytically, which, though a reasonable value, is much less than the PP of the heart.

3. Objectives

The primary objective of our current research is to study the effect of a two-layer fiber orientation on the Pumping Potential (PP) of the LV. Previously a single-layer near-conical FMC model of the LV was investigated, yielding an experimental and analytic PP of 1.67 and 1.9 respectively. Though a reasonable value, the PP of the single-layer near-conical FMC model is much less than the PP of the heart (or LV) which is 3.3-4. Consequently, we look at the effect of a more practical two-layer fiber orientation on the PP of the near-conical LV-like model. The PP of the near-conical two-layer LV-like FMC structure is investigated both experimentally and analytically.

4. Preliminary Work

A near-conical two-layer LV-like FMC structure is modeled to mimic the LV structure, and its Pumping Potential (PP) is investigated both numerically (ANSYS modeling) and experimentally. For both investigations, the modeling is based on the HVMB hypothesis (previously discussed in Section 2.2); that is, the heart is a made of a single band that twists and loops to form the ventricles. Consequently, we start with presenting the idealized band, the selection of the two-

layer fiber orientation, and the construction of the approximate near-conical shape of the LV. Then, we present the experimental and the finite element (ANSYS) work in Chapter 5.

4.1 Idealizing of Band Trace

Multiple goat hearts are dissected and unwrapped into HVMB, following the various dissection steps highlighted in the Section 2.2. Figure 34 display the endocardium (innermost layer), of one sample of the HVMB. The shape of the band (red line in Figure 34) is recorded and traced on a sheet of paper (Figure 36). Since we are only studying the LV, the RS (Right Section) of the basal loop, which forms the free wall of RV, is discarded. In addition, the LS (Left Section) is also ignored for the following reasons:

1. In the highly flexible LV structure, the LS is difficult to mimic using our Polyurethane (PU) band, because the PU is not as flexible and compliant as the heart muscle.

2. The LS is a small section adjacent the base of the LV, which is constrained in both our experimental and analytical models, and is consequently assumed to have a very small effect on the pumping action of the LV.

Figure 34: One sample of goat heart HVMB: Endocardium. The approximate LV band is traced using red line

The trace of the LV band is idealized (Appendix A) in order to engender a near-conical shape upon rolling and twisting. This idealization is accompanied by trimming the trace of the LV band into a circular sector with two radii. The schematic of creation of a conical structure from a simple circular paper sector (band) with two radii is shown in Figure 35. The red line (top edge) and the blue line (bottom edge) of the paper band form the base and the apex of the cone respectively. The crude LV band trace with the top edge (red line) and bottom edge (blue line) is shown in Figure 36. The idealized LV band is shown in Figure 37. The red stars are the band coordinate points recorded for using in analytical modeling of the LV band later.

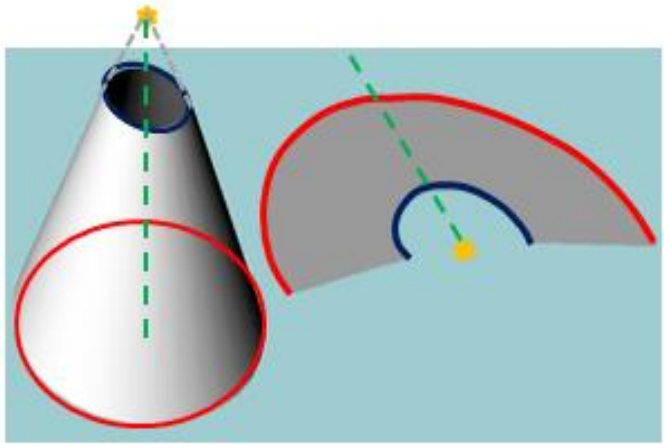

Figure 35: Sheet to cone formation. Red line and blue line represents the base and apex of the cone respectively. [38]

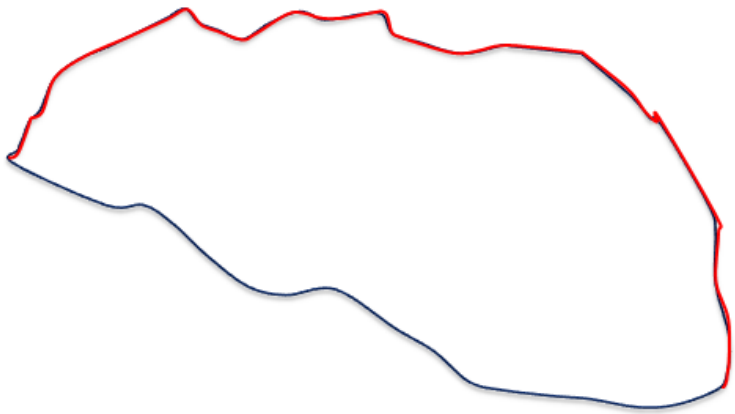

Figure 36: Crude LV band trace with top edge (red) and bottom edge (blue)

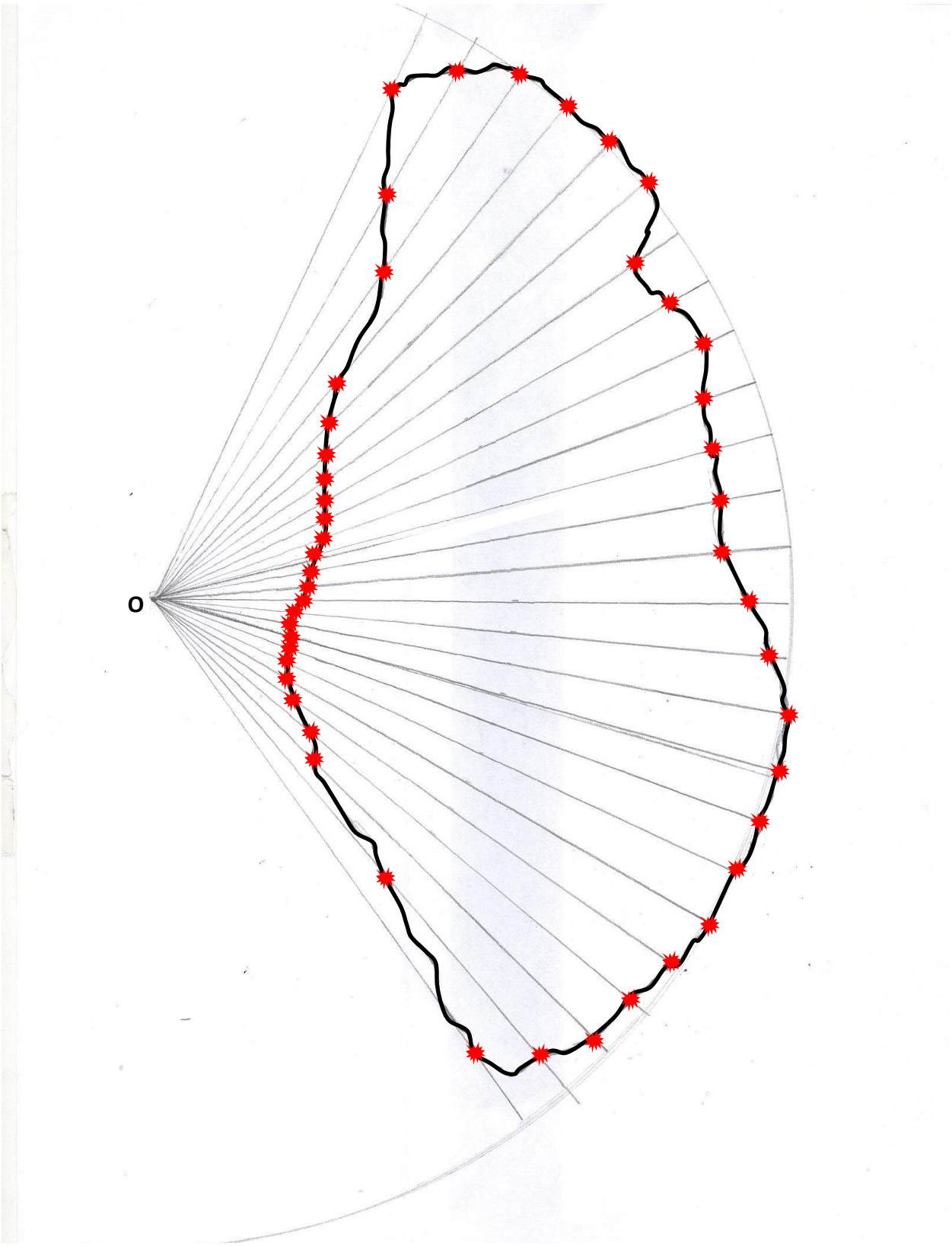

Figure 37: Idealized LV band trace. Red stars are band key-points recorded in polar coordinates

4.2 The Two-Layer Fiber Orientation

Our aim is to obtain the simplest and most practical fiber orientation in the LV, and to observe its effect on the PP of the twisted and looped near-conical LV-like structure. An analysis is conducted to see the effect of the fiber orientation of a simple asymmetric angle-ply conical structure on its PP. We assumed a cone of radius r and apex angle α, and found the volume change, ΔV, due to a change of the length of two input characteristic lines on the cone's surface, which makes an angle θ and - θ respectively with the slant height, s (Figure 38). The overall rotation was considered to be zero degrees due to the asymmetric angle-ply orientation adopted.

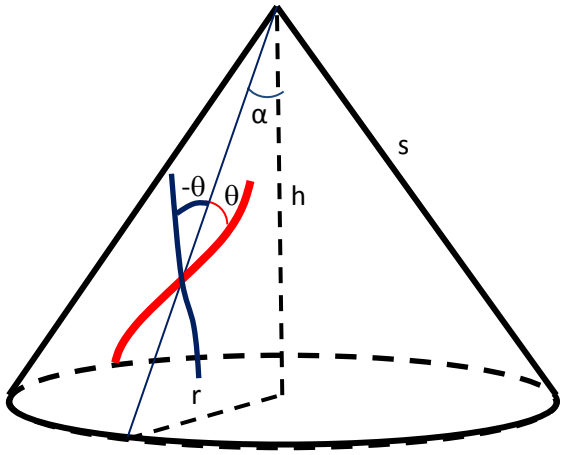

Figure 38: Parameters of the conical surface [9]

The volume, V, of the cone is

$$V(r,s) = \frac{1}{3}\pi r^2 h = \frac{1}{3}\pi r^2 \sqrt{s^2 - r^2} \qquad \text{(Equation 1)}$$

Where, r is the radius, h is the height and s is the slant height. Differentiating with respect to the two variable r and s, we get

$$\Delta V = \frac{2}{3}\pi r h\left(\frac{s^2 - 1.5r^2}{s^2 - r^2}\right)\Delta r + \frac{1}{3}\pi r^2\left(\frac{s}{h}\right)\Delta s,$$

Upon dividing by the volume (Equation 1), we get the expression for the volume reduction ratio:

$$\frac{\Delta V}{V} = 2\left(\frac{s^2 - 1.5r^2}{s^2 - r^2}\right)\frac{\Delta r}{r} + \left(\frac{s}{h}\right)^2\frac{\Delta s}{s} \qquad \text{(Equation 2)}$$

Introducing the following normal components of the strain: The tangential strain $\varepsilon_\theta = \Delta r/r$, the slant strain (along s) $\varepsilon_s = \Delta s/s$, the fiber's strain (along the characteristic length) $\varepsilon_l = \Delta L/L$, and ε_m normal to the characteristic line and along the surface of the cone. L is the length of the characteristic line. Applying the standard strain transformation, we have,

$$\begin{pmatrix}\varepsilon_s\\ \varepsilon_\theta\\ \varepsilon_{s\theta}\end{pmatrix} = \begin{bmatrix} m^2 & n^2 & 2nm\\ n^2 & m^2 & -2mn\\ -mn & mn & m^2 - n^2\end{bmatrix}\begin{pmatrix}\varepsilon_l\\ \varepsilon_m\\ \varepsilon_{lm}\end{pmatrix}, \qquad \text{(Equation 3)}$$

where $m = \cos\theta$, $n = \sin\theta$, and $\varepsilon_{s\theta}$ and ε_{lm} are the corresponding shear strain components. We assumed that the Poisson's effect is negligible, then when ε_l is imposed, we may impose $\varepsilon_m = \varepsilon_{lm} = 0$. Consequently, from (Equation 3):

$$\varepsilon_\theta = \frac{\Delta r}{r} = \frac{\Delta L}{L}\sin^2\theta, \text{and } \varepsilon_s = \frac{\Delta s}{s} = \frac{\Delta L}{L}\cos^2\theta$$

Substituting into (Equation 2), after some manipulation:

$$PP = \frac{\Delta V}{V}\Big/\frac{\Delta L}{L} = \left(2 - \tan^2\alpha\right)\sin^2\theta + \left(\sec^2\alpha\right)\cos^2\theta$$

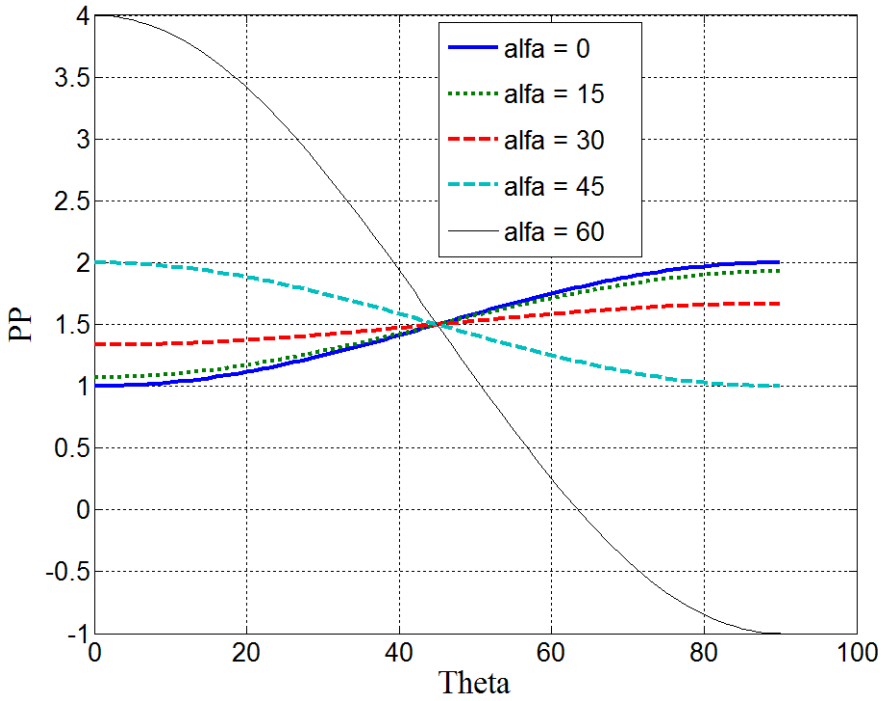

Figure 39: PP of the conical structure

The graph in Figure 39 displays PP versus θ for different values of the apex angle, α. The values of $\alpha > 45^{o}$ were found to be impractical for pumping, since the flexure stiffness of the cone's surface considerably abates and, therefore its pumping ability deteriorates as well. For values $\alpha < 45^{o}$, PP was found to be in the range of 1-2. Thus the expected range of PP for a simple asymmetric angle-ply conical structure is 1-2. However the LV, which is roughly a near-conical asymmetric angle-ply structure, shows a PP of 3.3-4 [1, 2]. Consequently the effect of the simplest and most practical two-layer fiber orientation on the PP of our near-conical LV-like structure is studied. The fiber orientation in the top most (epicardium) and bottom most (endocardium) layers of the HVMB of goat's heart is estimated via direct observation. The fiber orientation observed in the endocardium and epicardium layers of one sample of the HVMB is displayed in Figures 40 (A) and (B) respectively.

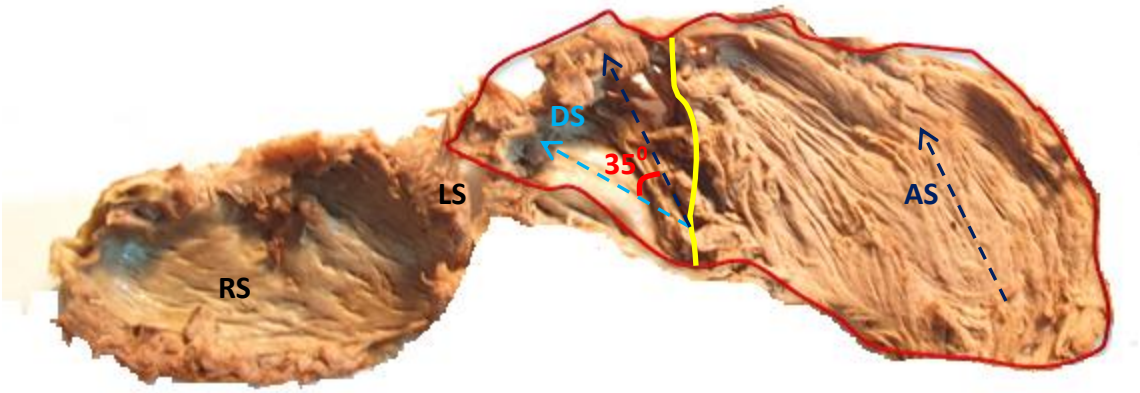

Figure 40 (A): Goat heart HVMB Endocardium: Two Main fiber directions (Sky blue and deep blue lines). The two regions in which these fiber orientations are observed, is separated by yellow line. The approximate LV band traced is shown using red line

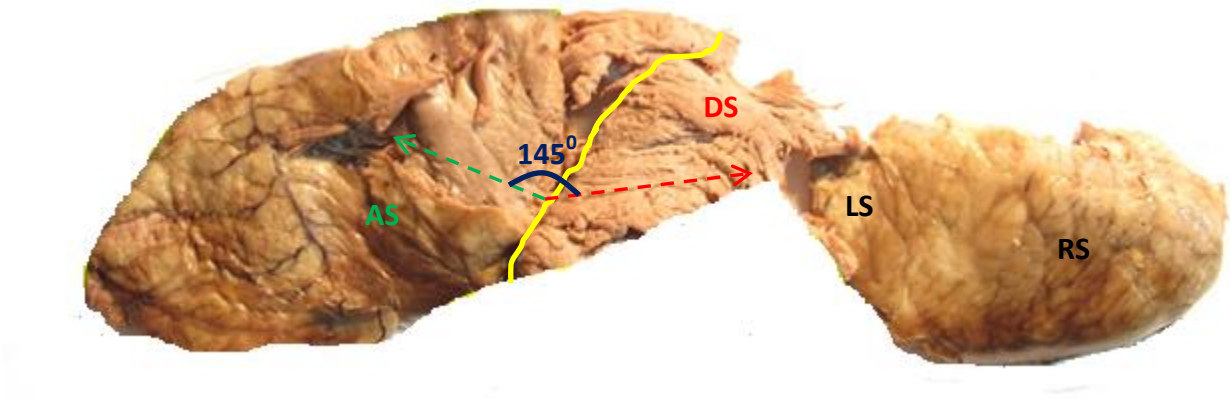

Figure 40 (B): Goat heart HVMB Epicardium: Two Main fiber directions (Green and red lines). The two regions in which these fiber orientations are observed, is separated by yellow line

Multiple goat hearts were dissected, and the fiber orientations observed in the two-layers of HVMB were compared with literature, to decide the idealized fiber orientation. The idealized band and two-layer fiber orientation is displayed in Figure 41.

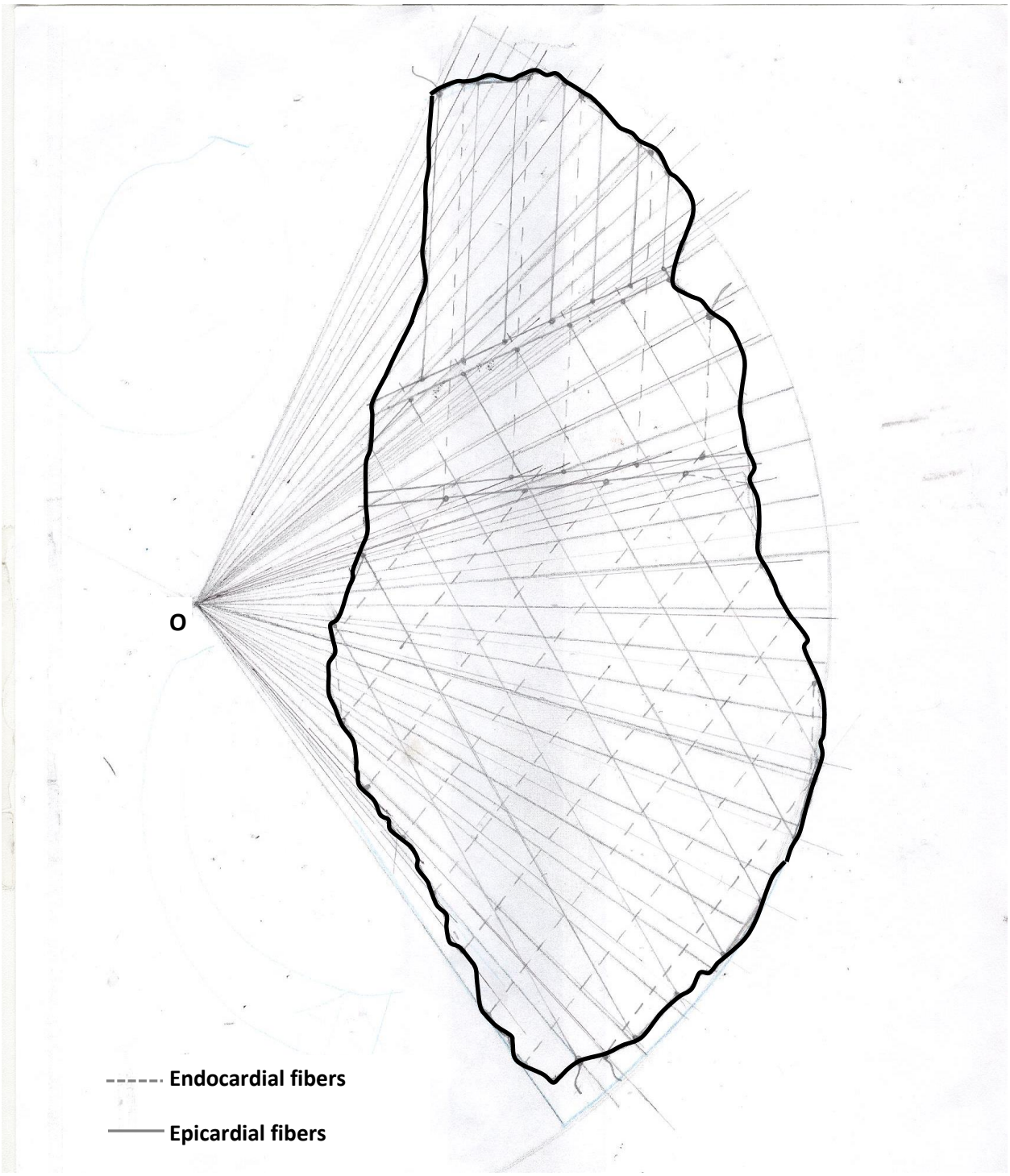

Figure 41: Idealized LV band trace with epicardial (hard lines) and endocardial (dashed lines) fiber lines.

4.3 Construction of Two-layer Near-Conical LV-Like FMC Structure

For both the experimental and finite element (FE) work, the construction of the two-layer near-conical LV-like model is accomplished by rolling the flat LV band (including the fibers) into a cone. Analytically, a Matlab code is written to roll each point of the band edges (top and bottom as shown in Figure 36) and fibers into the proper location on the cone. Experimentally, the flat band is manually rolled into the near-conical LV-like structure.

4.3.1 Experimental Construction

The construction of the two-layer near-conical LV-like FMC structure is done in two phases. In the first phase, an open Teflon mold (with depth of 0.3 cm) is prepared in house in the shape of the idealized LV band. Shape Memory Alloy (SMA) wires (used as actuating fibers) from Dynalloy ([40], .015' diameter, 5% maximum strain) are placed in the mold in two layers (Figure 42), guided by screws. The first layer of SMA wires are placed as per the recorded epicardial fiber orientation, followed by the layup of second (top) layer of SMA wires representing the endocardial fiber orientation. A suitable gap is maintained between the two layers, adjusted by the screw grooves, to avoid any possible short circuiting. Polyurethane resin (PU) is poured into the mold and left to cure for 8-10 hours (Figure 43). Once the curing is over, the screws are removed and the PU/SMA LV band (Figure 44) is taken out of the mold.

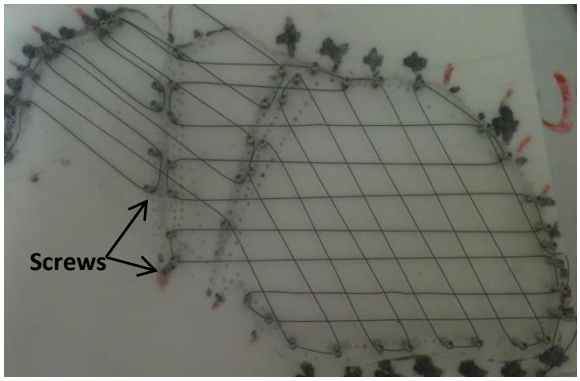

Figure 42: SMA wires placed in teflon mold

Figure 43: PU/SMA band in the mold

Figure 44: PU/SMA LV band

Figure 45: Near-conical LV like FMC model

In the second phase, the PU/SMA LV band (Figure 44) is twisted and looped (Section 2.2) to obtain the near-conical LV-like structure (Figure 45). The base of the conical structure is immersed into a bath of polyurethane to form a polyurethane base. The apex of the conical structure is shoved with a small tube extended out from the apex (Figure 45).

4.3.2 Analytical Construction

As mentioned above, analytically, the idealized band is rolled into the near-conical shape using a Matlab code. The input to Matlab is a set of points on the LV band edges (Figure 41). The rolling of the flat band surface into a cone is performed using the analysis described in Appendix B. The Matlab codes used for generating both the plots are provided in Appendix C. Figure 46 shows the idealized LV band plotted in Matlab. Figure 47 shows the rolled near-conical LV structure plotted in Matlab.

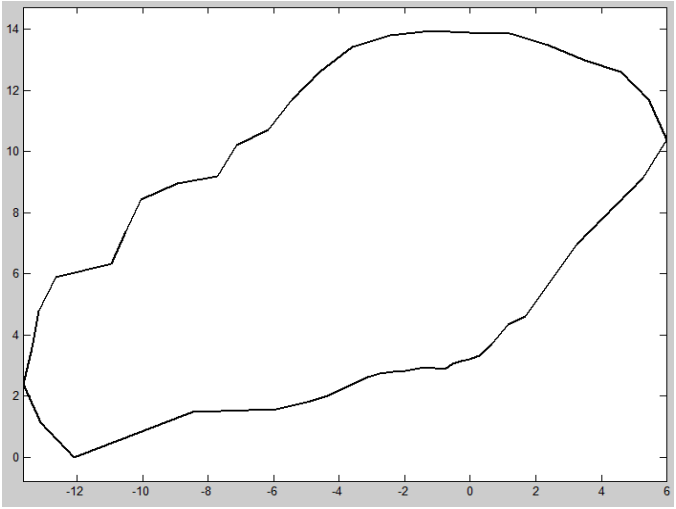

Figure 46: Idealized LV band trace plotted in Matlab

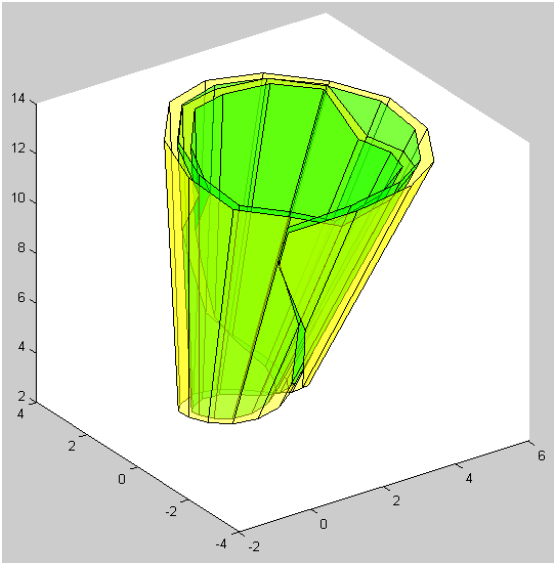

Figure 47: LV band rolled in Matlab

The epicardial and endocardial fibers points are plotted on the idealized LV band trace using a Matlab code (provided in Appendix C). In Figure 48, the red and blue colored lines represent the endocardial and epicardial fibers respectively. The fibers are rolled on to the near-conical LV-like structure using a Matlab code (Appendix C). The endocardial and epicardial fibers are located at 1/3rd thickness and 2/3rd thickness distance from the inner surface of the cone respectively. The near-conical LV-like structure with epicardial fibers (in blue color) and endocardial fibers (in red color) is presented in Figure 49.

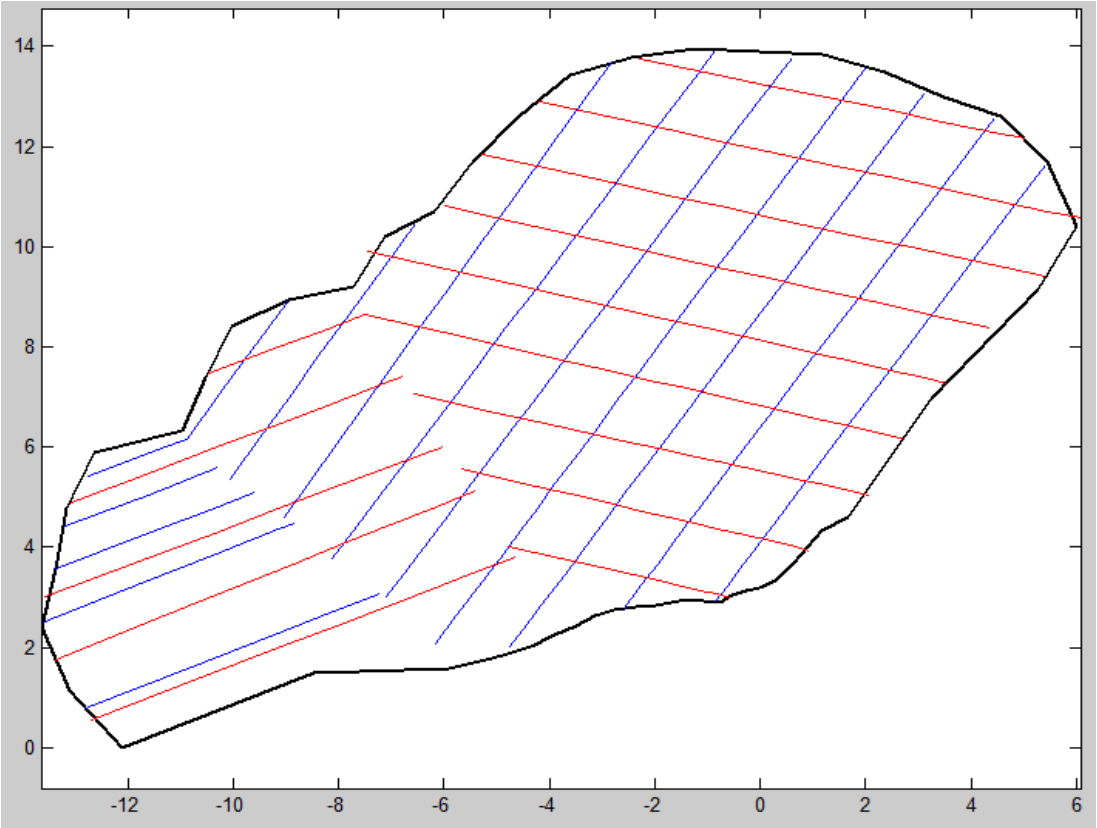

Figure 48: Idealized LV band with Epicardial (blue) and Endocardial (red) fibers plotted in Matlab

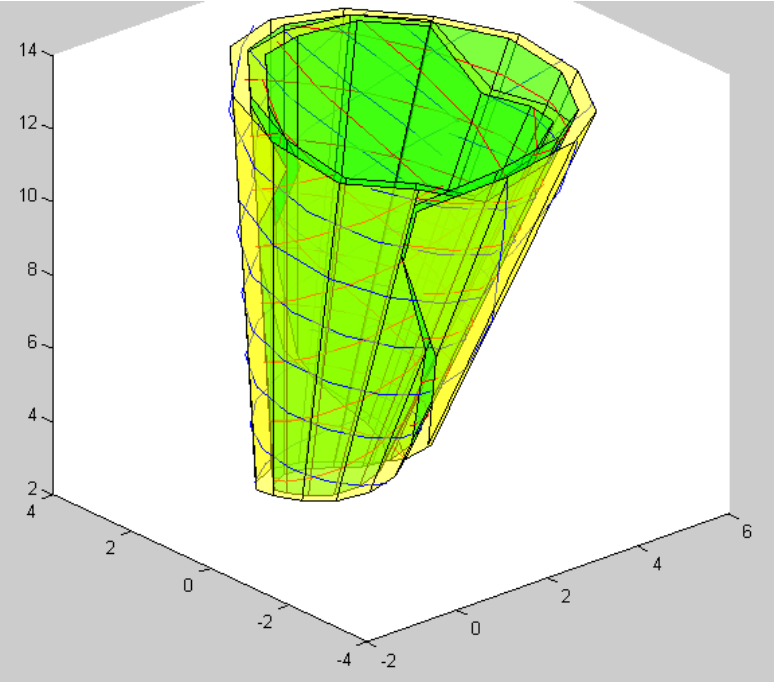

Figure 49: Near-conical LV-like structure with Epicardial (blue) and Endocardial (red) fibers rolled in Matlab

A closer look at the generated near-conical two-layer LV-like structure is presented in figure 50. It is noticed that there are two unique sides of the structure:

1. A septal or the Ascending/Descending side, which is made of two overlapping layers. The fiber orientations of the two layers are different. The two layers constitute an angle-ply laminate.
2. Non-septal side, which is constituted of three layers namely the ascending, descending and circumferential fiber orientation, again forming an angle-ply laminate.

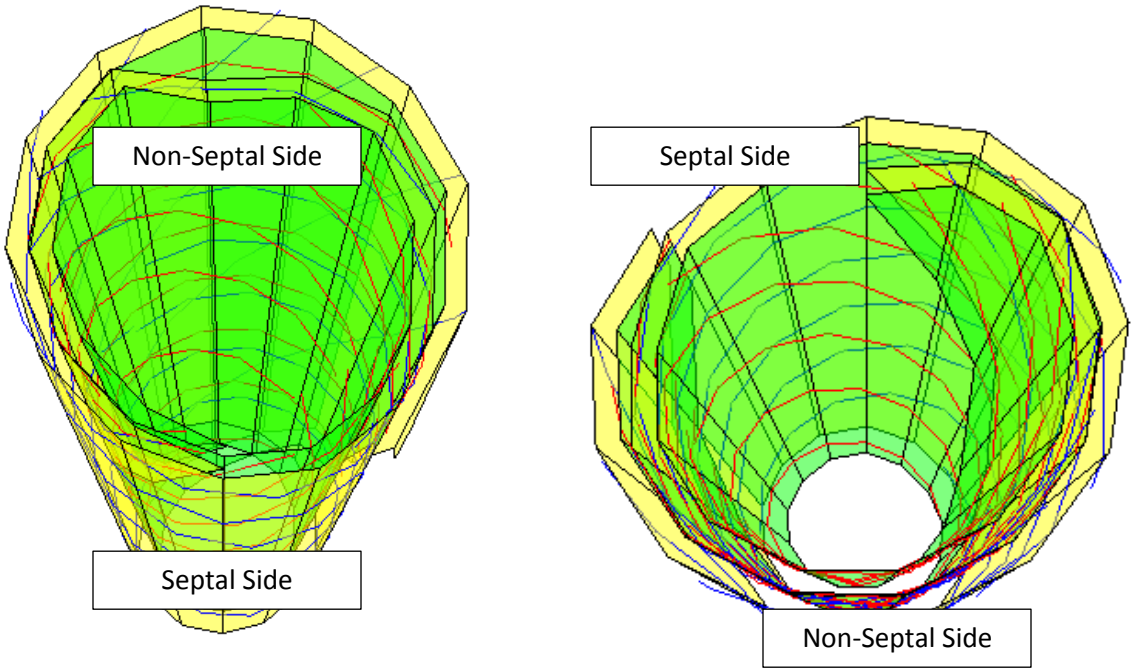

Figure 50: A closer look into the near-conical LV-like structure with Epicardial (blue) and Endocardial (red) fiber layers

Moreover the fiber angles measured in the two unique sides of the structure are:

1. Septal side: Approximately 60^{o} between Ascending and Descending fiber groups.
2. Non-septal side: Both the Ascending and Descending fibers approximately make opposite 60^{o} angles with the circumferential fibers. This observation has been previously reported in literature by Streeter et al, and has been mentioned in the literature section 2.1.

A Matlab code is used to write the rolled band and fiber points into a file (code provided in Appendix C). These points are used subsequently for modeling of the near-conical LV-like structure and the fibers in the epicardial and endocardial layers, in ANSYS.

5. Experimental and Analytical Work

In the experimental work, the experimental setup is prepared for computation of the PP of the near-conical two-layer LV-like structure. The analytical work section briefly presents the steps of modeling of the near-conical two-layer LV-like model in ANSYS and also the various modeling steps necessary (i.e. Creation of the inner volume, contact relations etc.) for computation of the PP.

5.1 Experimental Work

The SMA wires of the near–conical LV-like structure are connected to a power supply (GW Instek GPS-3303 Dual Output Linear DC Power Supply, 3 Channels, 3 Output Amps, 30 Output Volts, 195 Output Watts), and a plastic measuring tube is connected to the tube fixed to the apex of the conical structure, as shown in Figure 51. The structure is filled with water till the brim of the apex opening, and the SMA fibers are charged. As the fibers are activated and heated up, they contract, causing the structure to deform and to partially collapse inward, pumping out water up the extended measuring tube.

To estimate the PP of the near-conical LV-like FMC structure, the SMA is charged with the maximum allowed power, which generates the highest strain ($\Delta L//L_o$) in the SMA without destroying the shape memory of the wires. The volume of the displaced water (ΔV) in the extended tube is measured, and the PP of the near-conical LV-like FMC structure is computed.

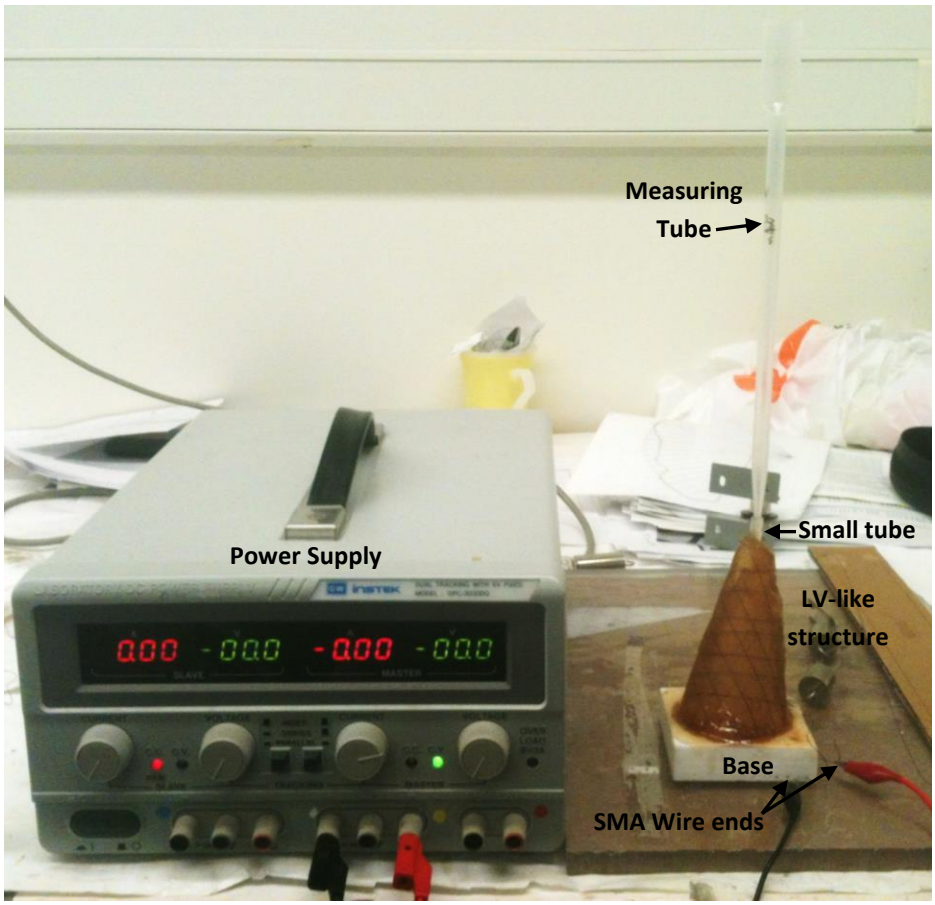

Figure 51: Experimental set-up

5.2 Analytical Work in ANSYS

The modeling of the near-conical LV-like FMC structure in ANSYS involves the following main steps:

1. The key-points are imported from Matlab, which represent the rolled LV band points for each of the inner and outer surfaces, and plotted in ANSYS workspace. In Figure 52, the red colored 1 and 25 points are the starting and end points respectively of the top basal outer surface of the cone. Similarly the green colored 1 and 25 points are the starting and end points respectively of the top basal inner surface of the cone.

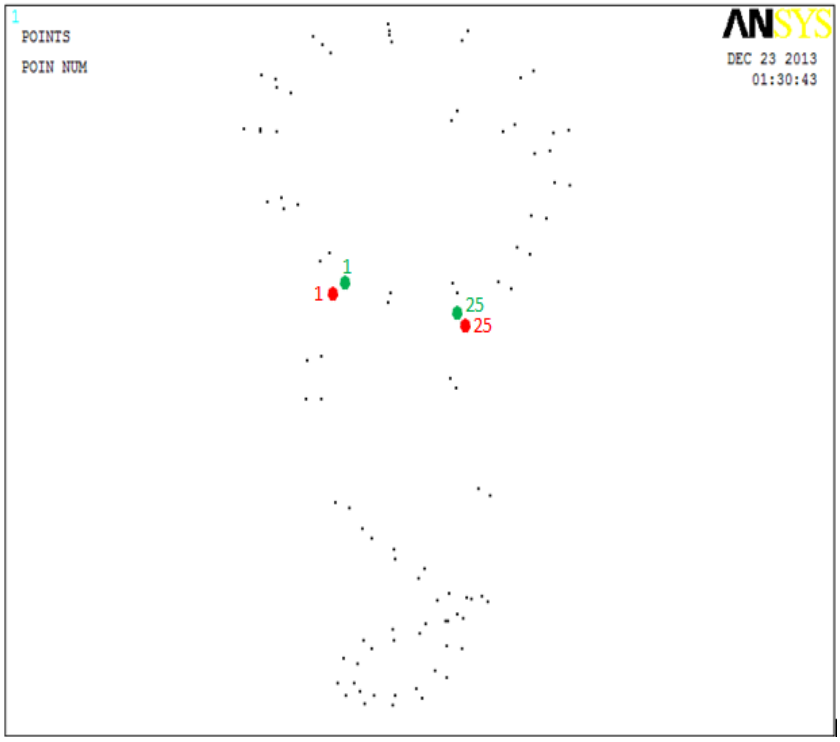

Figure 52: Rolled LV band key points plotted in ANSYS

2. The various key-points in Figure 52 are connected using splines and lines as shown in Figure 53 in different colors.

Figure 53: Rolled LV band lines plotted in ANSYS

3. The areas are created from lines in Figure 53. First, the top basal area (Red) in Figure 54 is created by using the two long basal splines (pink and purple) and two short ending lines (Yellow and Purple) in Figure 53. Secondly, the blue and purple rectangular areas are created (Figure 54). Thirdly, the green apical area is created by using the two long apical splines (green and pink) and the two small lines (blue and grey) in Figure 53. Next, the outer main surface (purple) is created by using the outer basal spline (pink), red and blue straight lines and outer apical spline (green) in Figure 53. The inner main surface is generated similarly. A total of six surfaces created can be visualized using Figure 54.

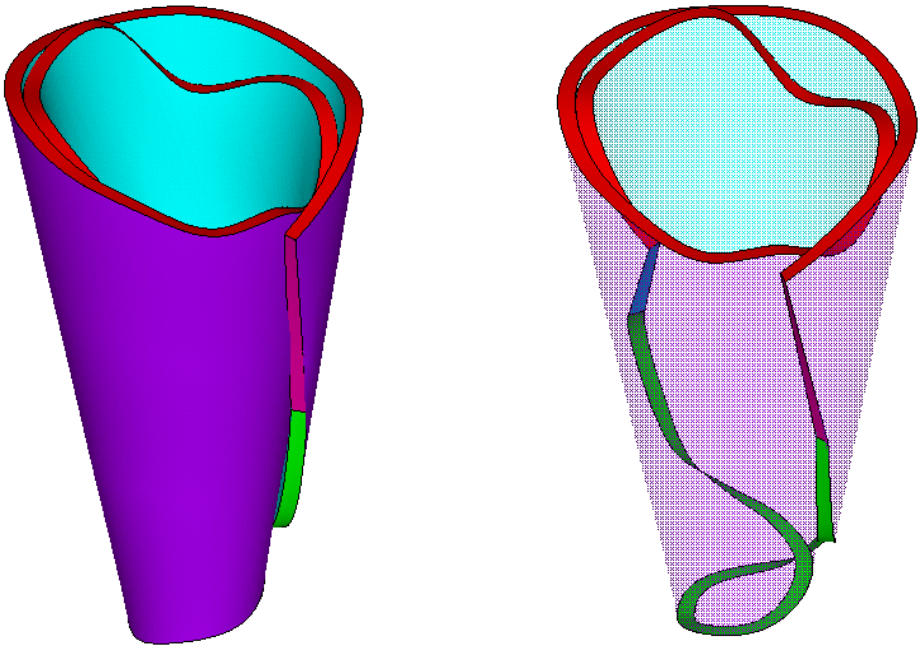

Figure 54: Two views of the rolled LV band areas plotted in ANSYS

4. The main volume (Figure 55) is created from areas in Figure 54. However due to difficulties (Appendix F) faced in subsequent meshing of the main volume, the main volume was subdivided into 24 sub-volumes as shown in Figure 56.

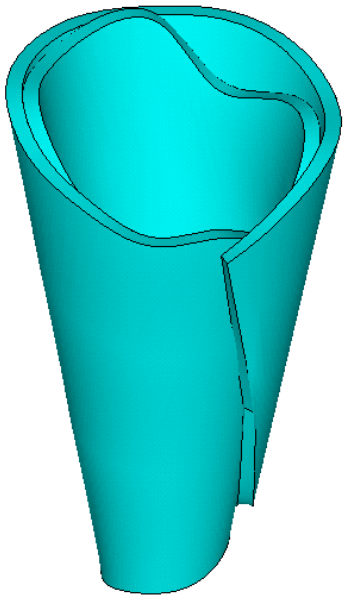

Figure 55: LV main volume

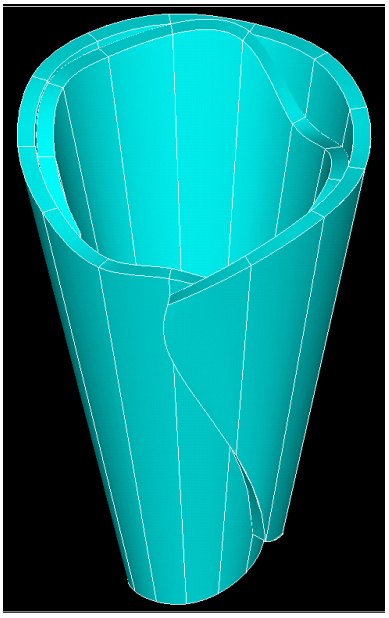

Figure 56: Subdivided LV main volume

5. The key-points representing the rolled fibers of the Epicardium (at 2/3rd thickness) and Endocardium (at 1/3rd thickness) are imported from Matlab and plotted in ANSYS. Each of the key-points are connected through B-splines to generate fiber lines. A sample of fiber line plotted in ANSYS is shown in Figure 57.

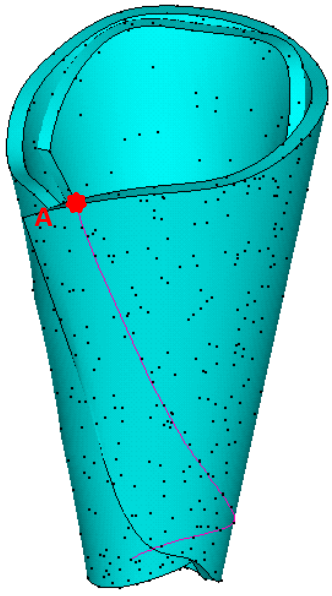

Figure 57: Single fiber spline plot

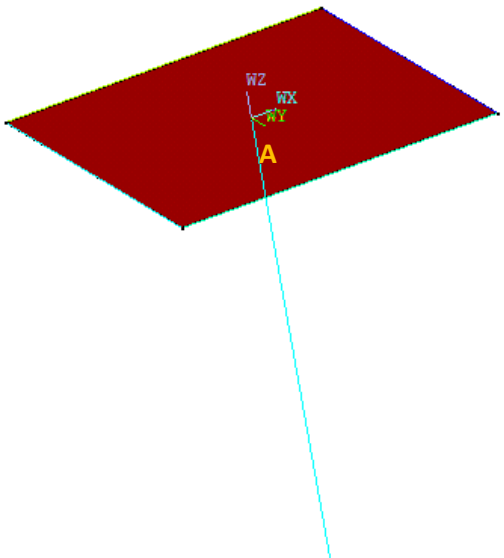

Figure 58: Area created normal to a fiber line

6. The fiber volumes with square cross-section are created by sweeping a square area (0.06 cm*0.06 cm) along every fiber line (Figure 58). Each of the fiber volumes are then divided into at least 3 sub volumes, to avoid meshing difficulties due to volume twisting (Appendix F). The square cross-section is adopted to limit the number of elements generated while meshing (mapped) (Figure 59).

Figure 59: Number of elements generated using mapped meshing in case of a square cross-section is much less than in case of circular cross-section

7. The fiber volumes are overlapped with the main LV volume using 'OVERLAP' operation. Figure 60 shows the fibers (blue) inside one main sub volume. Figure 61 shows the complex volume of a main sub volume, due to overlapping operation of the sub volume with fibers.

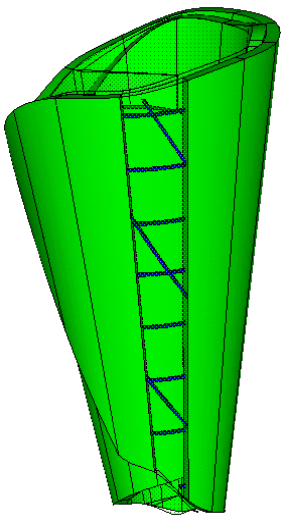

Figure 60: Fibers in a main sub volume

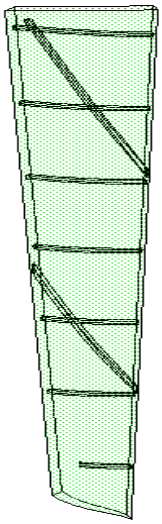

Figure 61: A main sub volume with embedded fibers

8. The common surface shared by the main sub volumes in blue and red colors in Figure 62, are bonded using contact–target pair elements as shown in Figure 63.

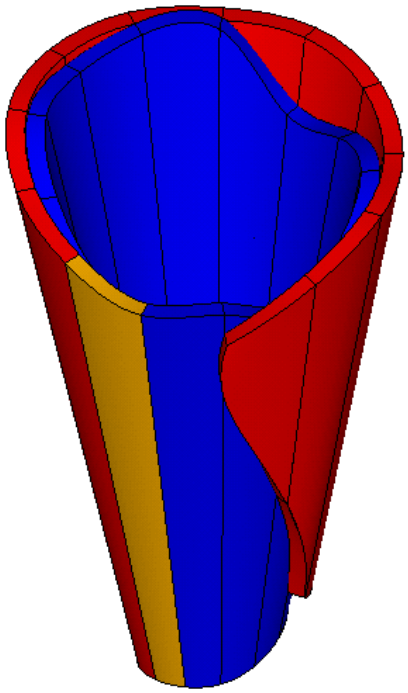

Figure 62: Volumes sharing common surface in LV main volume

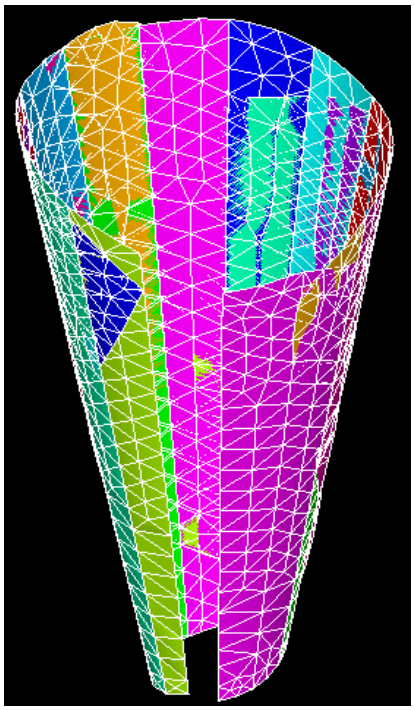

Figure 63: Contact-target pairing in main volume

9. An inner volume occupying the empty space inside the main LV volume is created to simulate the water (in experiments) in ANSYS. Consequently this inner volume will be used to quantify the percentage change in the volume of the empty space (ΔV/V %) inside the main volume, while the pumping is simulated. The complex process involved in the creation of this inner volume is discussed in Appendix D. Figures 64 (A, B) shows the different parts (in colors) of the inner volume.

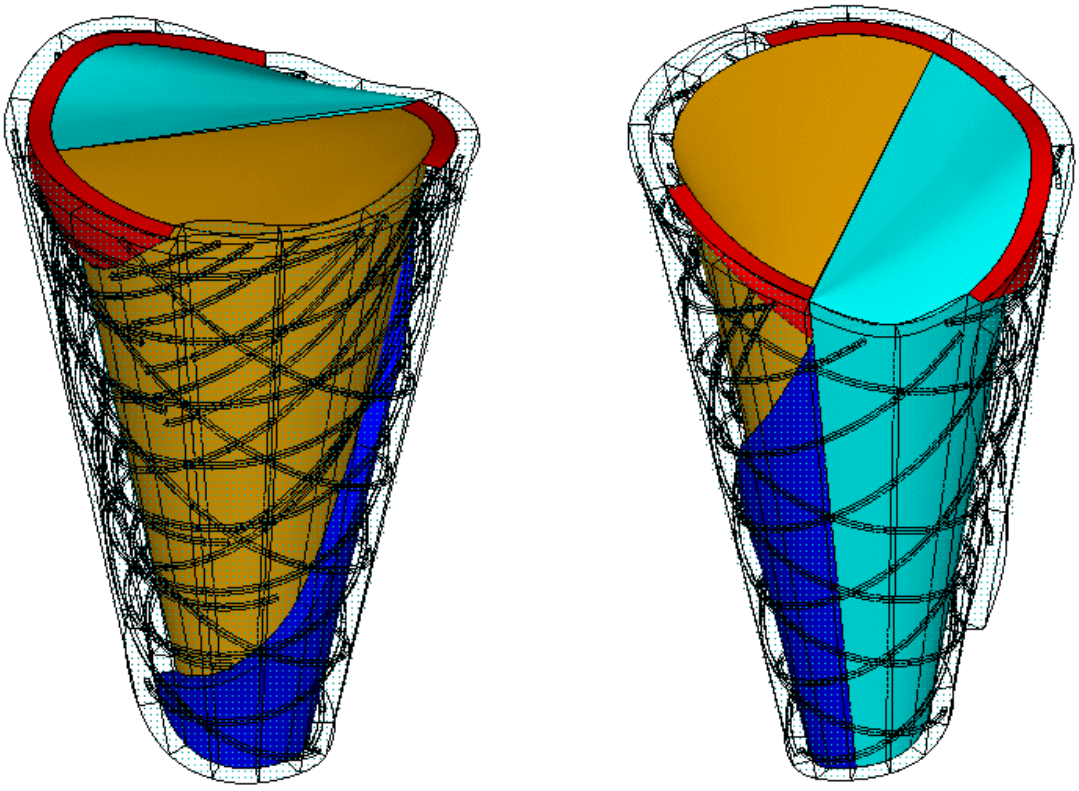

(A) (B)

Figure 64: (A) and (B) are two views of the different parts of the inner volume (in different colours), enclosed within the LV main volume (transparent).

10. The material properties for the Polyurethane (PU) LV main volume, SMA fibers and inner volume (core) are listed in Table 4. The element type selected is Solid 186 for the main volume, fibers and the inner volume.

Material	Property	Value	Unit
SMA	Modulus of Elasticity	133	GPA
	Poisson's ratio	0.33	
	Thermal Expansion coefficient	10^{-4}	K^{-1}
PU	Modulus of Elasticity	20	MPA
	Poisson's ratio	0.48	
Core	Modulus of Elasticity	1	KPA
	Poisson's ratio	0	

Table 4: Material properties for ANSYS

11. The finite element mesh is generated in three phases. First, the fibers are meshed using hex-mapped meshing technique and appropriate sizing controls. The mesh of the fibers is shown in Figure 65 (A), with epicardial fibers in yellow color and endocardial fibers in red color. Secondly, the Main LV sub volumes are meshed using tet-free meshing technique and with smart sizing '5'. The LV main volume mesh is shown in Figure 65 (B).

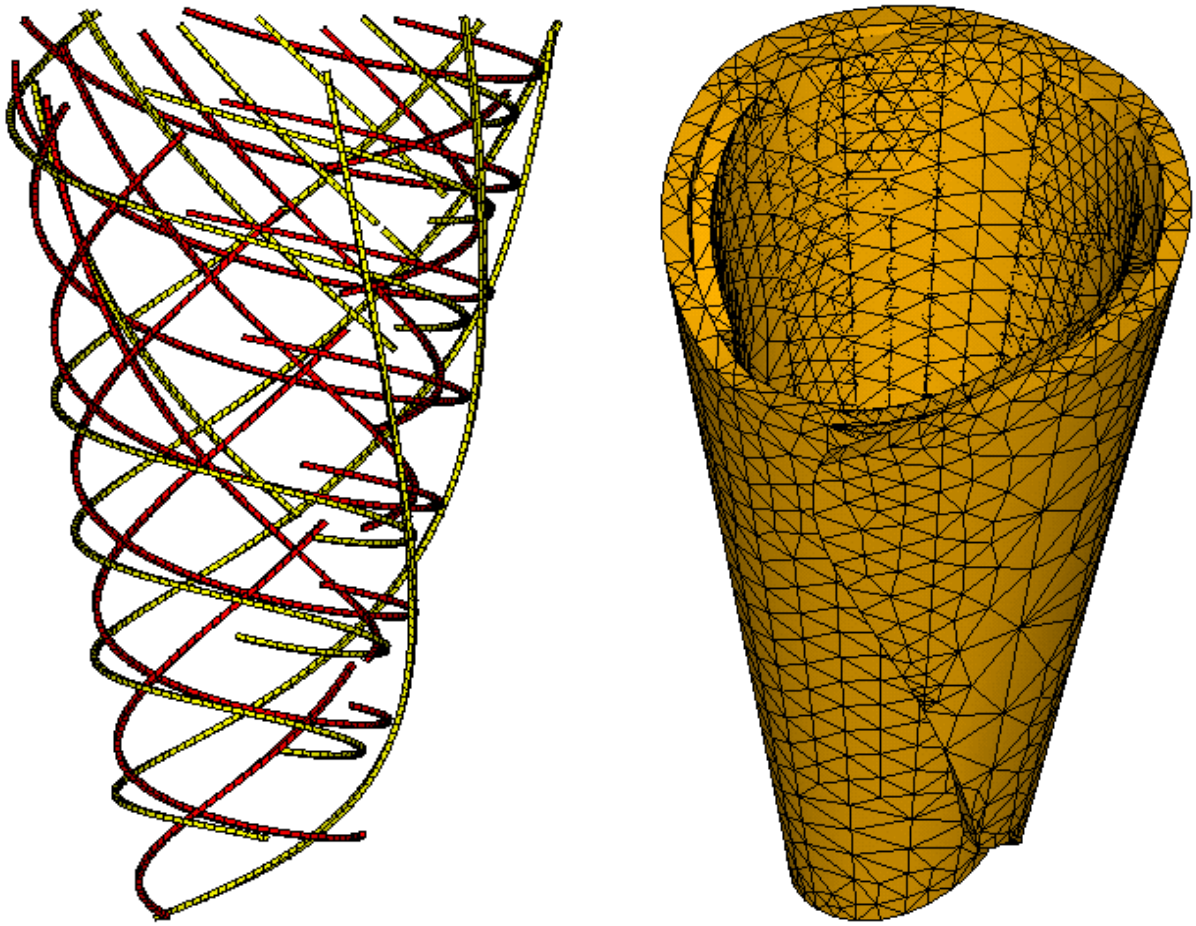

(A) (B)

Figure 65: (A) Epicardial (yellow) and Endocardial (red) fiber mesh. (B) Mesh of the LV main volume

Thirdly, the inner volume is meshed using tet-free meshing technique and with smart sizing 'Off'. The inner volume mesh is shown in Figures 65 (C, D). The main purpose of Figure 65 (D) is to show how well the inner volume mesh fits inside the main volume mesh (transparent). Some major difficulties faced while meshing are discussed in Appendix F.

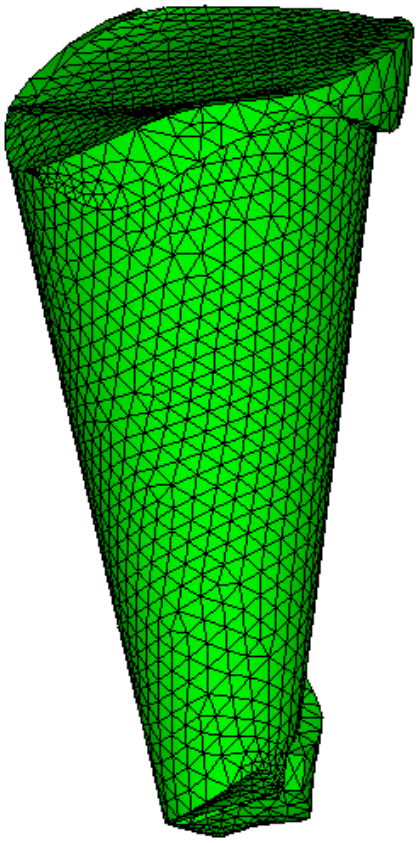

Figure 65 (C): Inner volume mesh

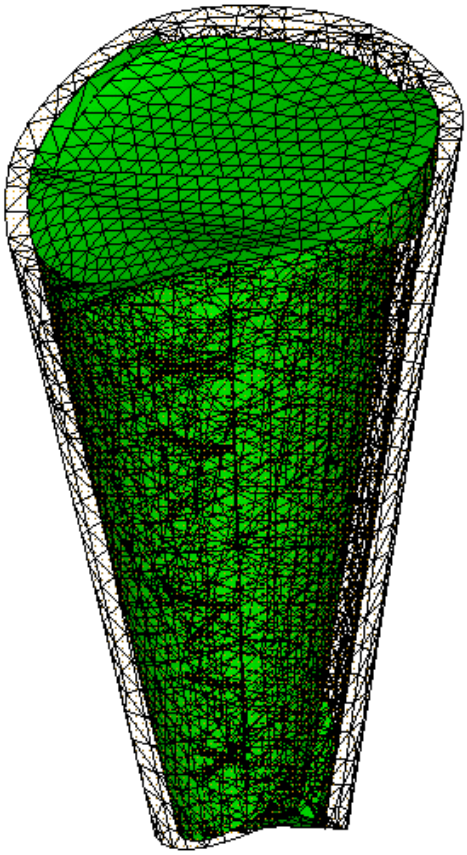

Figure 65 (D): Inner volume mesh inside main volume mesh (transparent)

12. The various parts of the inner volume are bonded together using contact-pairs. Also the inner volume is bonded with the main volume at the common surface using contact-pairs. Three contact-pair samples are shown in Figure 66.

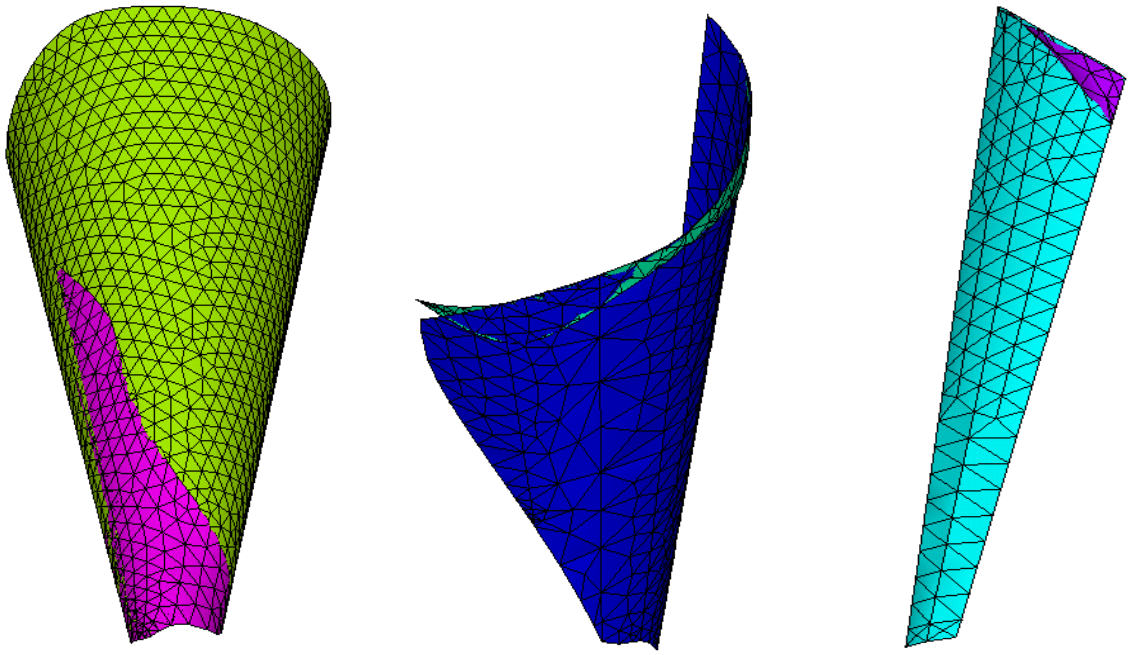

Figure 66: Contact-pairs involved in bonding of the inner volume parts with the main volume

13. Boundary conditions: The top basal surface of the near-conical LV-like model in ANSYS is constrained in all degrees of freedom (DOF's). All the fiber elements are thermally charged (indirectly using temperature loading) with 2% thermal strain.

14. A large deformation analysis is invoked and a non-linear solution is computed.

6. Results and Discussions

The pumping potential, defined as "the relative volume reduction engendered by an input stroke" [11, 12], of the simple and practical two-layer LV-like FMC structure is evaluated both experimentally and analytically.

6.1 Experimental Results

Experimentally, to estimate the PP of the near-conical LV-like FMC structure, the SMA is charged with the maximum allowed power, which generates the highest strain ($\Delta L//L_o$) in the SMA without destroying the shape memory of the wires. The volume of the displaced water (ΔV) in the extended tube is measured, and the PP of the near-conical LV-like FMC structure is computed using the following equation:

$$\textbf{\textit{Pumping Potential}}\ (\boldsymbol{PP}) = \frac{\frac{\Delta \boldsymbol{V}}{\boldsymbol{V_o}}\%}{\frac{\Delta \boldsymbol{L}}{\boldsymbol{L_o}}\%} \qquad \text{(Equation 4)}$$

Three experiments with five trials each were conducted. The results are summarized in Table 5. From the results, the average experimental PP is in the range of 2.73-2.95 approximately. The first trial (marked in red) is neglected in each experiment, because the SMA wire contracts under the maximum strain (approximately 4%) and undergoes a small amount of permanent hysteresis in the first trial. In the subsequent trials, the maximum SMA strain becomes consistent (approximately 3.6%).

Experimental Results					
	Parameter	ΔV(mL)	V_o(mL)	$\Delta L/L_o$(%)	PP
Experiment 1	Trial 1	7.5	61	4	3.07
	Trial 2	6.5	61	3.6	2.95
	Trial 3	6.5	61	3.6	2.95
	Trial 4	6.5	61	3.6	2.95
	Trial 5	6.5	61	3.6	2.95
Experiment 2	Trial 1	8	68	4	2.94
	Trial 2	7	68	3.6	2.85
	Trial 3	7	68	3.6	2.85

	Trial 4	7	68	3.6	2.85
	Trial 5	7	68	3.6	2.85
Experiment 3	Trial 1	7.5	66	4	2.84
	Trial 2	6.5	66	3.6	2.73
	Trial 3	6.5	66	3.6	2.73
	Trial 4	6.5	66	3.6	2.73
	Trial 5	6.5	66	3.6	2.73

Table 5: Experimental Pumping Potential (PP) results

6.2 Analytical Results

The deformation of the inner volume (ΔV) in the near-conical LV-like ANSYS model, under a thermal strain ($\Delta L//L_o$) in all the embedded fiber volumes, is calculated (Appendix E). The pumping potential (PP) is computed using the following equation:

$$\boldsymbol{Pumping\ Potential\ (PP)} = \frac{\frac{\Delta V}{V_o}\%}{\frac{\Delta L}{L_o}\%} \qquad \text{(Equation 4)}$$

The results are summarized in Table 6. The un-deformed and deformed mesh of the main LV volume, fibers and inner volume are shown in Figures 67, 68 and 69 respectively.

Analytical Results			
ΔV(mL)	V_o(mL)	$\Delta L/L_o$(%)	PP
4.6453	92.0594	2	2.5

Table 6: Analytical Pumping Potential (PP) results

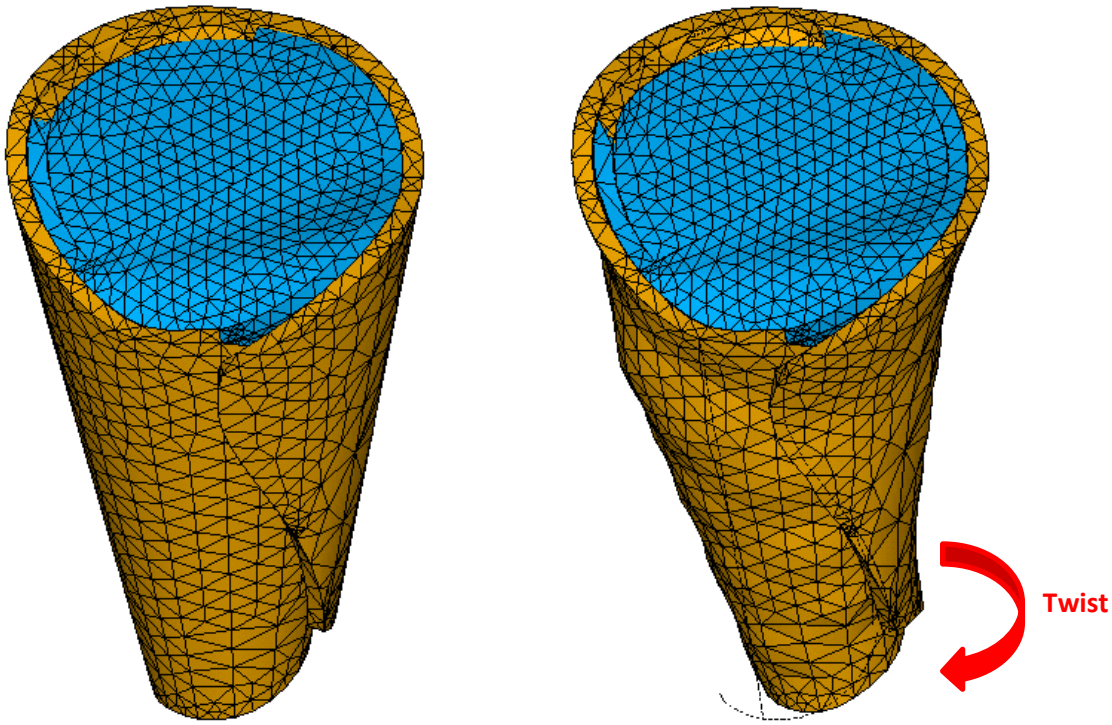

Figure 67: Main volume and inner volume mesh before (left) and after (right) deformation

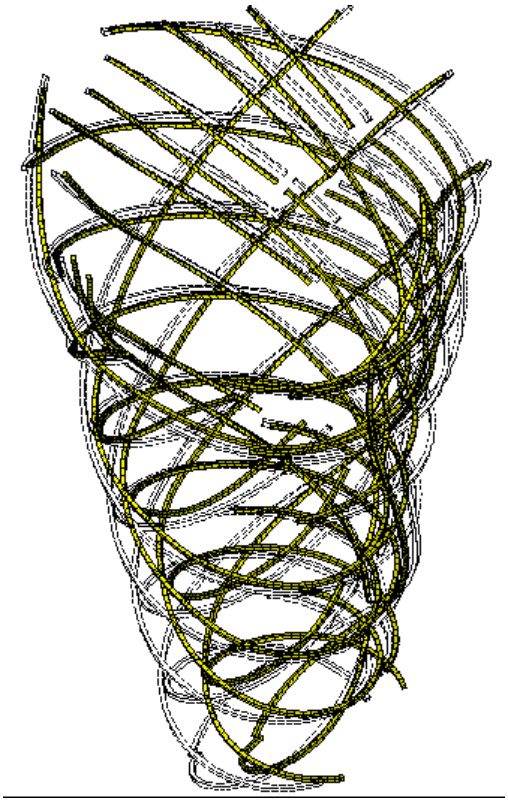

Figure 68: Fiber mesh deformed shape (yellow) and un-deformed edges (dashed black lines)

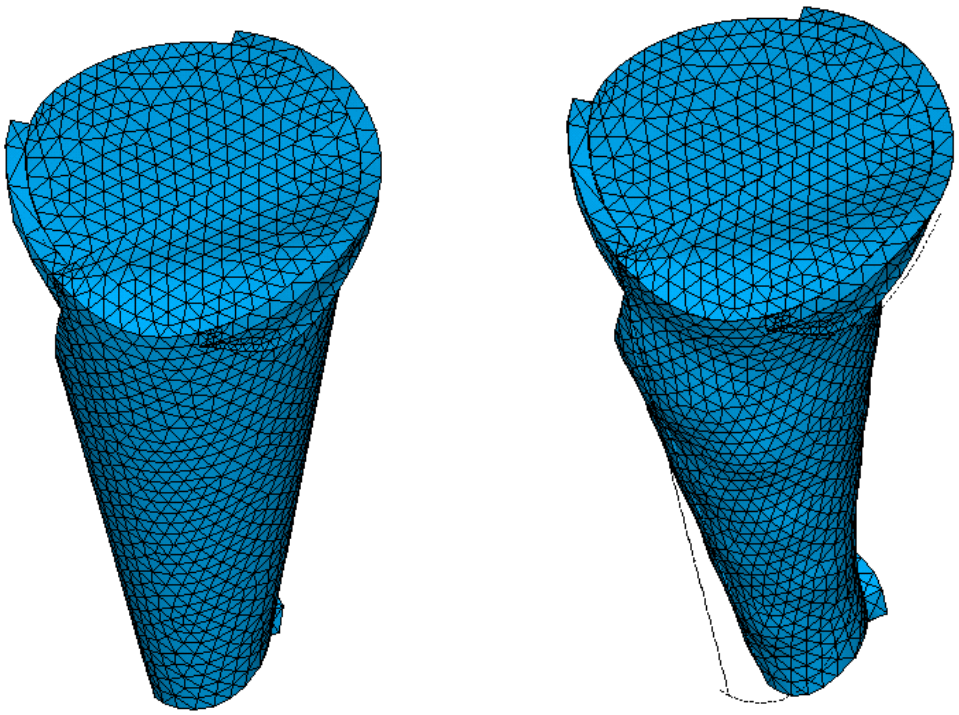

Figure 69: Inner volume mesh before (left) and after (right) deformation

Additionally, in the ANSYS animation, a clockwise ventricular apical twist [23] or wringing effect was observed clearly (also observed in Figure 67). Another effect observed was the thickening of the inner walls [41] (Appendix G) of the main volume. These effects have been previously pointed out in the literature and are believed to enhance the pumping efficiency of the LV.

7. Conclusions

The experimental and analytical investigation of the near-conical two-layer LV-like FMC structure yielded an average PP of 2.8 and 2.5 respectively. Though the PP is less than that of the heart's PP (3.3-4), compared to our previously investigated simple single-layer Left-Ventricle-

like FMC model, the PP has improved significantly, indicating that the fiber orientation in the heart plays an important role in defining its PP.

The difference between the PP of our near-conical two-layer LV-like FMC structure and the heart can be mainly attributed to the following reasons:

1. Idealized fiber orientation: A more accurate fiber orientation with a higher number of fibers should significantly improve the PP.
2. The material properties of the FMC (PU/SMA) adopted in our model are completely different from the biological properties of the heart's muscle, which may have a considerable effect on the PP, as previously observed in literature [43].
3. The boundary conditions are different. In our near-conical LV-like model, both in experiments and ANSYS, the base is fixed and the outer surface is free. This is different from the heart (Appendix H), in which, various structures such as the basal skeleton (no rotation [1]), apex (no translation along the long axis [1]), the pericardial sac (a conical sac of fibrous tissue surrounding the heart, which is radially stiff but circumferentially free [44]), and the atrial and ventricular valves constrain the myocardial motions [44, 45].
4. The strain application scheme on the fibers (single step), in our experiments and analysis, is different than that in the heart (multi step), which significantly affects the overall PP [1].

8. References

[1] Grosberg A., Gharib M., 2009, Computational models of heart pumping efficiencies based on contraction waves in spiral elastic bands, J. Theoretical Biology, Vol 257, pp. 359-370.

[2] Buckberg G.D., 2002, Basic science review: The helix and the heart, J Thorac and Cardio Surg, Vol 124, pp. 763-883.

[3] Aster J., Kumar V., Abbas A.K., Fausto N., 2005, Diseases of the white blood cells, lymph nodes, spleen and thymus, Robbins and Cotran pathologic basis of disease, Philadelphia, Elsevier Saunders, Ed. 7, pp. 661-695.

[4] http://www.britannica.com/blogs/2012/09/the-reptilian-nature-of-the-human-heart/

[5] http://www.efunda.com/formulae/solid_mechanics/composites/comp_intro.cfm

[6] Zdrahala R.J., Zdrahala I.J., 1999, Biomedical Applications of Polyurethanes: A Review of Past Promises, Present Realities, and a Vibrant Future, J. BiomaterAppl, Vol 14, pp. 67-90.

[7] http://www.fibre-reinforced-plastic.com/2010/12/lamina-and-laminate-what-is-that.html

[8] Hunter PJ, Borg TK. Integration from proteins to organs: the physiome project. Nat Rev Mol Cell Biol 2003; 4(3): 237—43.

[9] H. Ghoneim and A. Chanda,'Pumping Potential of a Left-Ventricle-Like Flexible-Matrix-Composite Structure', e-Proceedings of the 19th International Confer-ence on Composite Materials (ICCM19), Montreal Canada, 2013, pp: 7457-7462.

[10] Lawrie DJ, President, Lawrie Technology Inc., Girard, PA 16417, private communication.

[11] Ghoneim H., and Santos T., 2010, Evaluation of the Pumping Action of a Barrel-Shaped Composite Shell Structure, AmerSoc Mechanical Engineers, New York.

[12] Ghoneim H., and Noor S., 2012, Pumping potential of a hyperbolic shell-of-revolution flexible-matrix-composite structure, AmerSoc Mechanical Engineers, New York.

[13] Harvey W., 1628, An anatomical disquisition on the motion of the heart and blood in animals, In: Willis FA, Keys TE, eds. Cardiac classics. London: Henry Kimpton, 1941: 19-79.

[14] Kocica M.J., Corno A.F., Costa F.C., Rodes M.B., Moghbel M.C., Cueva C.N.C, Lackovic V., Kanjuh V., Guasp F.T, 2011, The helical ventricular myocardinal band; global, there-dimensional, functional architecture of the ventricular myocardium, Eur J CardiothoracSurg, Vol 29, pp. 21-40.

[15]Stensen N., 1664, De musculisetglandulisobservationum specimen, cum epistolisduabusanatomicis. Amsterdam:P le Grand, 90.

[16] Lower R., 1669, Tractatus de corde. London: J Allestry.

[17] Senac J.B., 1749, Traite de la structure du coeur. Paris: J Vincent.

[18]Ludwig C., 1849, Ueber den Bau und die Bewegungen der Herzventrikel. ZeitschriftfiurrationelleMedicin, Vol 7, pp. 189-220.

[19] MacCallum J.B., 1900, On the muscular architecture and growth of the ventricles of the heart. Johns Hopkins Hosp Rep, Vol 9, pp. 307-35.

[20] Mall F.P., 1911, On the muscular architecture of the ventricles of the human heart, Am J Anat, Vol 11, pp. 211-78.

[21] Streeter D.D., Spotnitz H.M., Patel D.P., Ross J., Sonnenblick E.H., 1969, Fiber orientation in the canine left ventricle during systole and diastole. Circ Res, Vol 24, pp. 339-47.

[22] Greenbaum R.A., Ho S.Y., Gibson D.G., Becker A.E., Anderson R. H., 1981, Left Ventricular Fiber Architecture in Man, Br Heart J, Vol 45, pp. 248-63.

[23] Nakatani, Satoshi. "Left ventricular rotation and twist: why should we learn?." Journal of cardiovascular ultrasound 19.1 (2011): 1-6.

[24] Gil D., Borras A., Ballester M., Carreras F., Aris R., Vazquez M., Marti E., Poveda F., 2009, MIOCARDIA: Integrating cardiac function and muscular architecture for a better diagnosis, In: proceeding of 14th International Symposium on Applied Sciences in Biomedical and Communication Technologies, Barcelona, Spain.

[25] WWW.Torrent-guasp.com

[26] Shan Y, Shan Y, Philen M, Lotfi A, Li S, Bakis CE, Rahn CD and Wang K-W. "Variable stiffness structures utilizing fluidic flexible matrix composites," Journal of Intelligent Material Systems and Structures. Vol. 20, pp 443-456, 2009.

[27] H. Ghoneim, "Investigation of the pumping action of a hyperbolic composite shell structure using the spline collocation method," Proceedings of the American Society for Composites, No. 028, 2007.

[28] Nielsen, P. M., et al. "Mathematical model of geometry and fibrous structure of the heart." American Journal of Physiology-Heart and Circulatory Physiology260.4 (1991): H1365-H1378.

[29] Dorri F., Niederer P.F., Lunkenheimer P.P., 2004, A finite element model of the human left ventricular systole, Computer Methods in Biomechanics and Biomedical Engineering, Vol. 9, pp. 319-341.

[30] Sermesant M., 2006, An Electromechanical Model of the Heart for Image Analysis and Simulation, Ph.D Thesis, Kings College, London, U.K.

[31] Vetter, Frederick J., and Andrew D. McCulloch. "Three-dimensional analysis of regional cardiac function: a model of rabbit ventricular anatomy." Progress in biophysics and molecular biology 69.2-3 (2005): 157-183.

[32] Wang T.T., 2008, Multi-Scale analysis of cardiac-myoarchitecture, Master's Thesis, Massachusetts Institute of Technology, Boston.

Link: http://dspace.mit.edu/handle/1721.1/45210

[33] Goktepe S., Acharya S.N.S., Wong J., Kuhl E., 2010, Computational modeling of passive myocardium, International Journal for Numerical Methods in Biomedical Engineering, Vol. 27, pp. 1-12.

[34] Holzapfel G.A., Ogden R.W., 2009, Constitutive modeling of passive myocardium. A structurally-based framework for material characterization, Philosophical Transactions of the Royal Society of London, Series A, Vol. 367, pp.3445–3475.

[35] Dokos S., Smaill B.H., Young A.A., LeGrice I.J., 2002, Shear properties of passive ventricular myocardium, Am J. of Physiol (Heart Circ. Physiol.), Vol. 283, pp. 2650–2659.

[36] Trayanova, Natalia A. "Whole-heart modeling applications to cardiac electrophysiology and electromechanics." Circulation Research 108.1 (2011): 113-128.

[37] Torrent-Guasp, Francisco FESC, W. F. Whimster, and K. Redmann. "A silicone rubber mould of the heart." Technology and Health Care 5.1 (1997): 13-20.

[38] http://www.mettleworks.com/graphics/cone.jpg

[39] Kocica, Mladen J., et al. "The helical ventricular myocardial band of Torrent-Guasp." Seminars in Thoracic and Cardiovascular Surgery: Pediatric Cardiac Surgery Annual. Vol. 10. No. 1. WB Saunders, 2007.

[40] http://www.dynalloy.com/pdfs/TCF1140.pdf

[41] Mitchell J.H., Wildenthal K., Mullins CB., 1969, Geometric studies of the left ventricle utilizing biplane cinefluorography, Fed Proc, Vol 28, pp. 1334-43.

[42] Spotnitz H.M., Sonnenblick E.H., 1976, Structural conditions in the hypertrophied and failing heart. In: Mason DT, editor. Congestive heart failure. New York: Yorke Medical Books; pp. 13-24.

[43] Guccione, J. M., A. D. McCulloch, and L. K. Waldman. "Passive material properties of intact ventricular myocardium determined from a cylindrical model." Journal of biomechanical engineering 113.1 (1991): 42-55.

[44] Wong, Ken CL, et al. "Meshfree implementation of individualized active cardiac dynamics." Computerized Medical Imaging and Graphics 34.1 (2010): 91-103.

[45] Mechanics and Material Properties of the Heart using an Anatomically Accurate Mathematical Model, PhD thesis, University of Auckland, 1998.

Link: https://researchspace.auckland.ac.nz/handle/2292/84

9. Appendices

Appendix A: Idealizing of LV band

The crude LV band trace is idealized by trimming the trace (along black dashed line in Figure 70) into a circular sector with two radii. The starting (Red) and ending (Blue) lines of the band are also decided. The aim is to have the starting and ending edges as straight and simple as possible, which will subsequently simplify the modeling of the near-conical LV-like FMC structure.

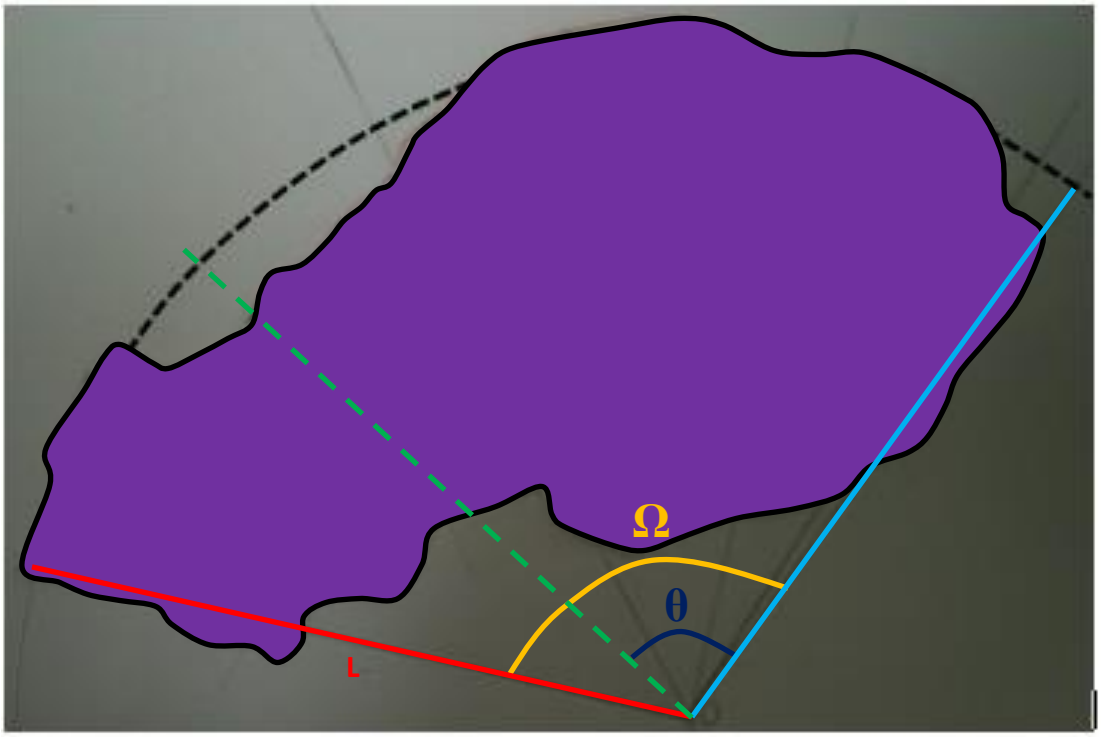

Figure 70: LV paper band trace. Red line: Starting line, Blue line: Ending line of the idealized band. Ω is the total band angle and θ is the angle subtended by the band for one conic rotation

Additionally, the radius and band spin for the resulting near-conical structure is determined, which will be subsequently used as inputs to the Matlab codes for rolling the band and fibers:

Angle subtended by the conic section for one rotation of cone: θ

Total angle subtended by the Band: Ω.

Band Spin= Ω / θ

Radius of cone (r): Arc length of band constituting one complete conical rotation=Circumference of the cone

$$2\pi L * \frac{\theta}{360} = 2\pi r$$

Appendix B: Rolling a plane surface into a conical surface

The rolling of the flat band surface into a cone with a known apex angle and the associated fibers in the two layers across the thickness of the cone is performed using the analysis described below [9].

As shown in Figure 71, we place the flat surface on the YZ plane. The target cone is placed such that the Z-axis coincides with one of the cone's side (slant) line, and that the axis of the cone, defined by the unit vector **w**, lies in the XZ plane.

Let us assume a generic point on the flat plane, A_1, which is to be moved to the corresponding point A_3 on the surface of the target cone. Also, let us denote $\mathbf{R_1}$ and $\mathbf{R_3}$ as the vector representations of points A_1 and A_3, respectively. The transformation of point A_1 to A_3 is accomplished via two consecutives rotations of the vector $\mathbf{R_1}$. The first rotation, which renders $\mathbf{R_2}$, is achieved by rotating the vector $\mathbf{R_1}$ about the X-axis with an angle Ψ. In the second rotation, the vector $\mathbf{R_2}$ is rotated about the unit vector of the axis of the cone **w** by an angle, θ, such that RΨ = r θ, where R is the magnitude of the vector $\mathbf{R_i}$ (i = 1, 2 or 3) and r is the radius of the cone

at the intermediate point A_2 (Figure 71). Note that r = R sin α, where α is the apex angle of the cone.

It can be shown that the transformation matrix **T**, which rotates $\mathbf{R_2}$ about **w** producing $\mathbf{R_3}$, is given by

$$\mathbf{R_3} = \mathbf{T} \cdot \mathbf{R_2},$$

where $\mathbf{T}(\mathbf{w}, \theta) =$

$$\begin{bmatrix} w_x w_x vc + c & w_y w_x vc - w_z s & w_z w_x vc + w_y s \\ w_x w_y vc + w_z s & w_y w_y vc + c & w_z w_y vc - w_x s \\ w_x w_z vc - w_y s & w_y w_z vc + w_x s & w_z w_z vc + c \end{bmatrix}$$

with c = cosθ, s = sinθ, and vc = 1 - cosθ. The angle cosines w_x, w_y and w_z are of the unit vectors **w**; that is, $\mathbf{w} = (w_x, w_y, w_z)^T$.

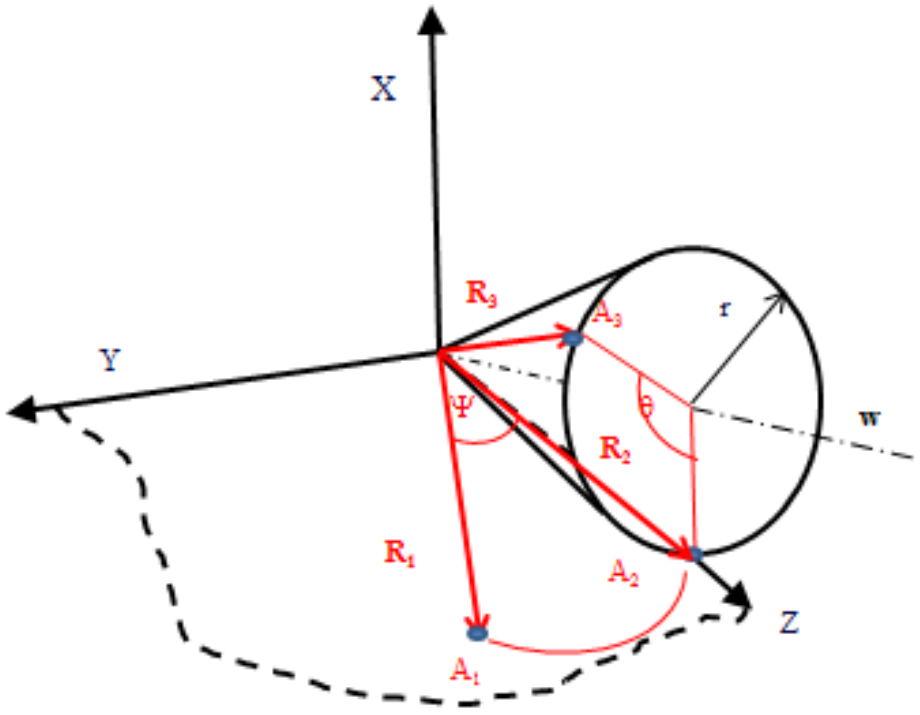

Figure 71: Schematic illustration of the rolling process of a flat plane into a conical surface. [9]

It should be also mentioned that r, while generating the near-cone LV-like structure, is increased in proportion to θ, such that the incremental increase in r every complete revolution (θ = 2π) equals to the thickness of the flat plate. This way, the excess portion of the flat plane with θ > 2π wraps perfectly well over the previously rolled portions with θ < 2π; that is, without any gaps between the two mating surfaces.

Appendix C: Matlab codes for LV band, fibers and LV-like model generation

1. LV band plotting

```
% Flat Band
% The flat portion in the y-z plane
% n ... number of points along the length
% m ... number of points along the width
% Factor ... rate of increasing the spin angle
% rr ... Radius of the cone's base (Any one)
% RR ... Corresponding Radius of the flat band
% ang_rev ... required looping angle
% Rr ... is RR/rr
ang_rev=1.846; Total Spin Angle
conv   = pi/180;
thickness=0.3; Band Thickness
%.............................................................
%BAND LAYUP
% R is in cm
R = [12.1 12.1; 13.15 10; 13.85 8.6; 13.85 6.1; 14 5.3; 13.95
4.8; 12.65 4.5;12.85 4.25; 13.1 4.1; 12.65 3.9; 12 3.65; 12.45
3.45; 12.35 3.35; 12.9 3.25; 13.4 3.1; 13.9 3; 14 3.1; 14 3.15;
13.9 3.2; 13.9 3.35; 13.7 3.75; 13.45 4.5; 13.4 4.9;12.9 7.7; 12
10.55]; Polar end coordinates of band points at every 5 degrees
ang   = [0:5:120]; Measurement at every 5 degrees, Band=120°
[n m] = size(R);
mxang = max(ang);
psi   = conv*[ang' ang'];
Rr    = ang_rev*360/mxang;
z     = R.*cos(psi);
y     = R.*sin(psi);
% Plot original Band after adjustment
tmp(:,1) = z(:,1);
```

```
tmp(:,2) = z(n:-1:1,2);
x_band     = tmp(:);
tmp(:,1) = y(:,1);
tmp(:,2) = y(n:-1:1,2);
y_band   = tmp(:);
% Close the plot
x_band(2*n+1) = x_band(1); Last point plot=starting point
y_band(2*n+1) = y_band(1);
%subplot(1,2,1);
plot(-x_band,y_band,'k','LineWidth',2)
axis equal
```

---

2. LV band rolling

```
% Roll into cone
% Needed spin angle, rr*spin = RR*psi
% For pure cone: RR = 1, rr = 0.25
% Unit vector of the axis of the cone w = [wx wy wz]
psix = atan(1/Rr);
wy   = 0;
wz   =   cos(psix);
wx   =   sin(psix);
% The Transformation matrix about cones axis Rw
% Then rotate just the edge with the appropriate spin
% Notice that the edge is local z coordinates
% Define an edge point (with x=y=0)
% kk is for the number of surfaces
%    includes the midsurfaces of the fibers
**********************
for kk = 1:3 Thickness divided into three surfaces
for jj = 1:m
for ii = 1:n
    Rij  = R(ii,jj);
    psij = psi(ii,jj);
    spin = psij*Rr;
    % Rotational matrix
    % To rotate a vector, passing by the origin, about the spin
axis
    Ctt = cos(-spin);
    Stt = sin(-spin);
    Vtt = 1 - Ctt;
    Vt  = Vtt;
    Ct  =  Ctt;
    St  = Stt;
    Rw  = [wx*wx*Vt+Ct    wy*wx*Vt-wz*St   wz*wx*Vt+wy*St;
           wx*wy*Vt+wz*St wy*wy*Vt+Ct      wz*wy*Vt-wx*St;
```

```
            wx*wz*Vt-wy*St wy*wz*Vt+wx*St   wz*wz*Vt+Ct];
    % Consider the gradual change in thickness
    % Just drop the reference axis and elongate
    % xR  = psij*thickness*((kk-1)+1/mxangr);
    % zR  = Rij*(1+thickness*((kk-1)+1/sin(psix)));
    xR  = thickness*((kk-1)/2+spin/(2*pi));
    dzR = xR*tan(psix);
    zR  = Rij+dzR;
    pm = [-xR 0 zR];
    pc(ii,jj,:) = Rw*pm';
end
end
xx = pc(:,:,1);
yy = pc(:,:,2);
zz = pc(:,:,3);
%subplot(1,2,2);
% Notice that (xxk,yyk,zzk) are for ANSYS plotting;
if kk == 1
    surf(xx,yy,zz,'facecolor','green');
    xx1 = xx;
    yy1 = yy;
    zz1 = zz;
    hold on
% elseif kk == 2 Middle surface not plotted
%     surf(xx,yy,zz,'facecolor','yellow');
%     xx2 = xx;
%     yy2 = yy;
%     zz2 = zz;
elseif kk == 3
    surf(xx,yy,zz,'facecolor','yellow')
    xx3 = xx;
    yy3 = yy;
    zz3 = zz;
end
axis square
alpha(0.5)  % For transperancy <0:1>
end
```

---

3. Fiber plotting and rolling

```
%PLOTTING FIBERS
%-------------------------------------------------------------
-----------
% Record and plot fibers
%EPICARDIUM.....................................................
.....................
```

```
% Data_fiber: R1 R2 Th1 Th2 N_points location_across_thikness
%n_layers = 1;
n_fibers = 14; Number of fibers in the epicardium
hh = thickness;
Rt = [3.05 12.85 74 115 10; ... |(115-74)/5|+1=Number of fiber
3.8 13.35 47 109.5 14; ...      points=10
5.15 13.45 23 103.5 18; ...
6.5 13.75 18.5 98.5 17;...
7.7 13.8 23 92.5 15;...
8.95 13.95 25 86.5 14;...
10.15 14 27 78.5 12;...
11.4 12.35 28 58 7;...
12.5 12.65 29.5 45 5;...
13.85 12.5 23 29.5 3;...
13.9 11.7 18.5 28.5 3;...
13.85 10.85 15 28 4;...
13.8 9.9 10.5 27 5;...
12.85 7.85 3.5 23 5;...
];

%hh = thickness/(n_layers+1);
% Planar coordinates of fibers
%  with intersection with the longitudinal lines
%  m1 = (y2-y1)/(z2-z1) = (y-y1)/(z-z1)
% nj ... number of points/fiber, multiple of the longitudinal
span
% 5  ... increment between two latitudes (degree)
mt = 1;
dT = 5/mt;
R1 = Rt(:,1); R2 = Rt(:,2);
T1 = Rt(:,3); T2 = Rt(:,4);
nj = Rt(:,5);
z1 = R1.*cos(T1.*conv);
y1 = R1.*sin(T1.*conv);
z2 = R2.*cos(T2.*conv);
y2 = R2.*sin(T2.*conv);
mf = (y2-y1)./(z2-z1);
% Find intersecion & Rotate fibers
% Equation of longitudinal: y = m2*x
hl = hh;
for ii = 1:n_fibers
nji = nj(ii);
mfi = mf(ii);
T1i = T1(ii);
T2i = T2(ii);
z1i = z1(ii); z2i = z2(ii);
y1i = y1(ii); y2i = y2(ii);
```

```
m1  = mfi;
num = - m1*z1i + y1i;
for jj = 1:nji
    if jj == nji
        Tij = T2i;
    else
        Tij  = T1i + dT*(jj-1);
    end
    psij = Tij*conv;
    if psi/conv == 90
    zij = 0;
    else
    m2   = tan(psij);
    dum  = m2 - m1;
    zij = num/dum;
    end
    yij     = m2*zij;
    Rij     = sqrt(yij^2+zij^2);
    xfj(jj) = - zij;
    yfj(jj) = + yij;
    Rf(jj)  = Rij;
    psf(jj) = psij;
    spin    = psij*Rr;
    % Rotational matrix
    % To rotate a vector, passing by the origin, about the spin
axis
    Ctt = cos(-spin);
    Stt = sin(-spin);
    Vtt = 1 - Ctt;
    Vt  = Vtt;
    Ct  =  Ctt;
    St  = Stt;
    Rw  = [wx*wx*Vt+Ct    wy*wx*Vt-wz*St   wz*wx*Vt+wy*St;
           wx*wy*Vt+wz*St wy*wy*Vt+Ct      wz*wy*Vt-wx*St;
           wx*wz*Vt-wy*St wy*wz*Vt+wx*St   wz*wz*Vt+Ct];
    % Consider the gradual change in thickness
    % Just drop the reference axis and elongate
    % xR  = psij*thickness*((kk-1)+1/mxangr);
    % zR  = Rij*(1+thickness*((kk-1)+1/sin(psix)));
    xR  = thickness*((2/3)+spin/(2*pi)); Gradual spin
    dzR = xR*tan(psix);
    zR  = Rij+dzR;
    pm = [-xR 0 zR];
    pf(jj,:) = Rw*pm';
end
% Plot fibers on Heart
subplot(1,4,3)
```

```
xfb = pf(1:nji,1);
yfb = pf(1:nji,2);
zfb = pf(1:nji,3);
plot3(xfb,yfb,zfb)
For checking
if ii == 3
xf_check = xfb;
yf_check = yfb;
zf_check = zfb;
end
% Plot fibers on Band
subplot(1,4,4)
xfk = xfj(1:nji);
yfk = yfj(1:nji);
plot(xfk,yfk)
end

%ENDOCARDIUM
%-----------------------------------------------------------------
-----------
% Record and plot fibers
%.....................................................................
...........
% Data_fiber: R1 R2 Th1 Th2 N_points location_across_thikness
%n_layers = 1;
n_fibers = 14;
hh = 0;
Rt = [13.95 13.15 80.5 112.5 8; ...
13.55 12.2 72 120 11; ...
12.95 10.85 66 120 12; ...
12.35 9.45 61 117.5 13;...
12.4 8.1 53 116 14;...
11.45 6.75 49 114 14;...
9.65 5.45 47 112.5 15;...
7.95 4.05 44.5 103.5 13;...
6.25 3.05 40 79.5 9;...
12.7 6 2.5 39.5 8;...
13.5 7.45 7.5 43.5 9;...
13.9 8.5 12.5 45 8;...
13.95 10.05 20.5 47.5 7;...
12.85 11.45 35.5 49 4;...
];
```

Rest all code remains the same as in case of Epicardium, except the following step: Because the endocardial fibers are plotted at 1/3rd of the thickness distance from the band inner surface.

```
    xR  = hl+thickness*((1/3)+spin/(2*pi));
```

---

4. Writing rolled band and fiber points into files for ANSYS plotting

---

```
% ---For ANSYS plotting---
% Inner-surface of Band
npt = [1:n];
Tmp = [npt' xx1(:,1) yy1(:,1) zz1(:,1)];
MM1 = Tmp';
fid = fopen('Surf1_Edge1','w');
fprintf(fid,'%8.0f  %14.4f  %14.4f %14.4f\n', MM1);
fclose(fid);
Tmp = [npt' xx1(:,2) yy1(:,2) zz1(:,2)];
MM1 = Tmp';
fid = fopen('Surf1_Edge2','w');
fprintf(fid,'%8.0f  %14.4f  %14.4f %14.4f\n', MM1);
fclose(fid);
% Outer-surface of Band
npt = [1:n];
Tmp = [npt' xx3(:,1) yy3(:,1) zz3(:,1)];
MM1 = Tmp';
fid = fopen('Surf2_Edge1','w');
fprintf(fid,'%8.0f  %14.4f  %14.4f %14.4f\n', MM1);
fclose(fid);
Tmp = [npt' xx3(:,2) yy3(:,2) zz3(:,2)];
MM1 = Tmp';
fid = fopen('Surf2_Edge2','w');
fprintf(fid,'%8.0f  %14.4f  %14.4f %14.4f\n', MM1);
fclose(fid);
%ANSYS band Plotting done-------------------------------
%ANSYS Fiber Plotting Epicardium-------
npf = [1:nji];
Tmf0 = [npf' xfb yfb zfb];
if ii == 1
    Tmf = Tmf0;
else
    Tmf = [Tmf; Tmf0];
end

% np_total = sum(nj);
% nptc     = [1:np_total];
% Tmf(:,1) = nptc';
MM2 = Tmf';
fid = fopen('epifibers','w');
fprintf(fid,'%8.0f  %14.4f  %14.4f %14.4f\n', MM2);
fclose(fid);
```

```
end
```

Similarly the endocardium fiber points are also written in a separate file.

Appendix D: Inner volume key-point plotting in Matlab

To create the inner volume key points, the original band is modified as explained below. These modified points along with the original key points were connected accordingly to create the inner volume parts using bottoms up approach:

1. The original 25 band points (in polar coordinate system), which were rolled to obtain the LV main volume key points are as follows:

```
R = [12.1 12.1; 13.15 10; 13.85 8.6; 13.85 6.1; 14 5.3;
13.95 4.8; 12.65 4.5; 12.85 4.25; 13.1 4.1; 12.65 3.9; 12
3.65; 12.45 3.45; 12.35 3.35; 12.9 3.25; 13.4 3.1; 13.9 3;
14 3.1; 14 3.15; 13.9 3.2; 13.9 3.35; 13.7 3.75; 13.45 4.5;
13.4 4.9; 12.9 7.7; 12 10.55];
```

   The LV like model in ANSYS and the actual rolled band is revisited in Figure 72 and 73 respectively. In Figure 72, the rolled band inner surface starts at inner point 1 and ends at outer point 25. If point 1-11 is changed to points 14-24 respectively, rest all points remaining the same, the base becomes flat with the inner and outer top edges parallel to each other. This is done in step 2.

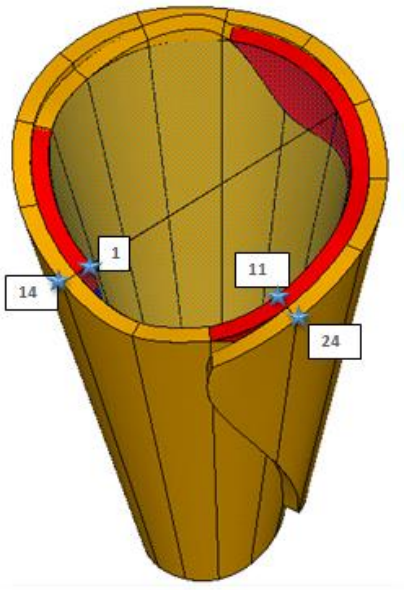

Figure 72: LV volume with inner sub-volumes

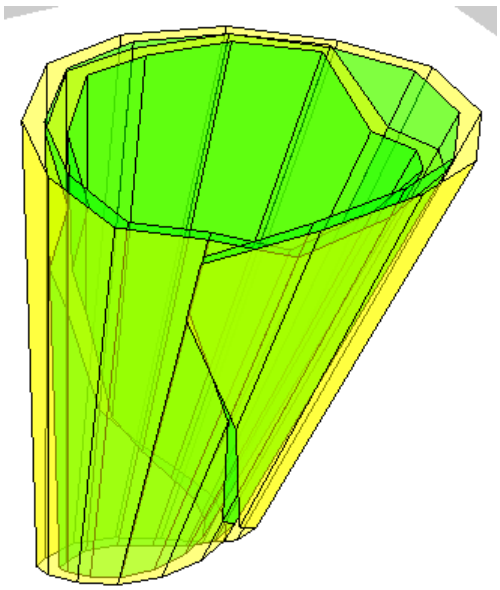

Figure 73: LV near-conical structure revisited

2. New rolled band points are plotted by feeding the following input to Matlab:

```
R = [12.9 3.25; 13.4 3.1; 13.9 3; 14 3.1; 14 3.15; 13.9
3.2; 13.9 3.35; 13.7 3.75; 13.45 4.5; 13.4 4.9; 12.9 7.7;
12.45 3.45; 12.35 3.35; 12.9 3.25; 13.4 3.1; 13.9 3; 14
3.1; 14 3.15; 13.9 3.2; 13.9 3.35; 13.7 3.75; 13.45 4.5;
13.4 4.9; 12.9 7.7; 12 10.55];
```

The points in red color are the changed input points. The resulting rolled band is presented in Figure 74.

3. To make the apex flat with the inner and outer bottom edges parallel to each other, few input points (in red) are changed as follows:

```
R = [12.9 3.25; 13.4 3.1; 13.9 3; 14 3.1; 14 3.15; 13.9
3.2; 13.9 3.35; 13.7 3.75; 13.1 4.1; 12.65 3.9; 12 3.65;
12.45 3.45; 12.35 3.35; 12.9 3.25; 13.4 3.1;13.9 3; 14 3.1;
14 3.15; 13.9 3.2; 13.9 3.35; 13.7 3.75; 13.45 4.5; 13.4
4.9;12.9 7.7; 12 10.55];
```

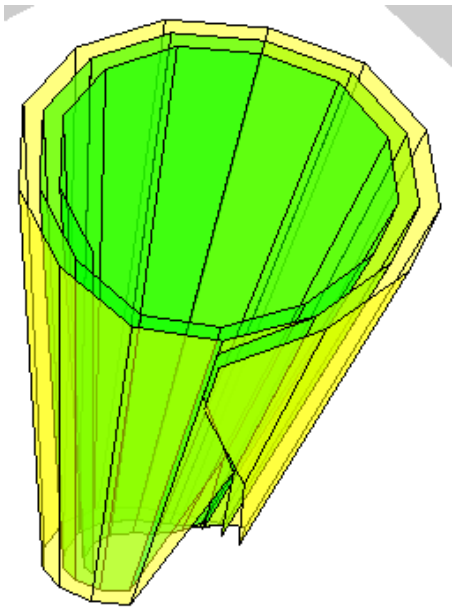

Figure 74: Flat base of near-conical LV-like model

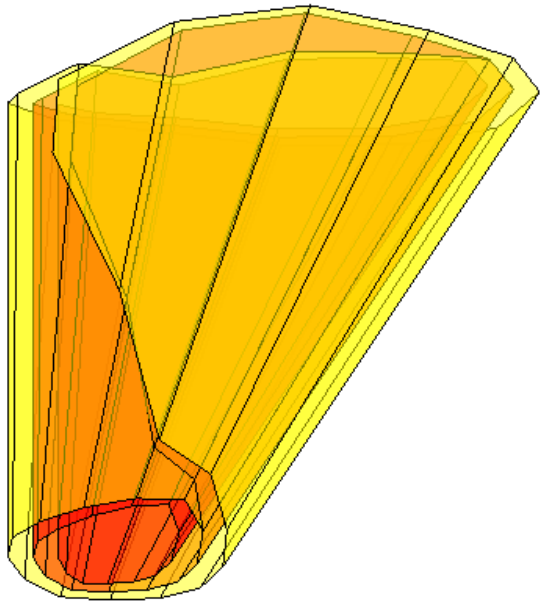

Figure 75: Flat apex of near-conical LV-like model

The resulting rolled band apex is shown Figure 75. The new rolled band points for the base and apex are plotted in ANSYS and connected with the old LV main volume key points using splines/lines. The lines are subsequently converted into areas and areas into various parts of the inner volume.

Appendix E: ANSYS GUI commands

1. Creating key points:

Preprocessor→Modeling→Create→Key points→In active CS→(X, Y, Z) key point coordinates

2. Creating lines from key points:

Preprocessor→Modeling→Create→Lines→Splines→Through Key points→ Select key points

3. Creating areas from lines:

Preprocessor→Modeling→Create→Areas→Arbitrary→By lines→ Areas made using 4 lines

4. Creating volumes from areas:

Preprocessor→Modeling→Create→Volumes→Arbitrary→By Areas→ Volume made using 6 surfaces

5. Main volume meshing:

1. Preprocessor→Element Type→Add/Edit/Delete→Add→Solid 186
2. Preprocessor→Material Props→Material Models→Add→Structural→Linear→Elastic→ Isotropic→Ex=2000, Prxy=.48
3. Preprocessor→Meshing→Mesh Tool→Select Tet, Free→Mesh→Select volume

6. Creating fiber volumes from splines:

1. Defining a coordinate system normal to the spline (at red star location A) using the GUI command: Work plane→ Align WP with→ Plane normal to line→Pick the fiber spline→Ratio along line=0
2. Creating an area perpendicular to the spline at point A, using the GUI command: Preprocessor→Modeling→Create→Areas→Rectangle→By Centr & Cornr→Select point A (It should show the location as 0,0)→Width=0.06, Height=0.06→OK
3. Sweeping the area along the spline to create the fiber volume, using the GUI command: Preprocessor→Modeling→Operate→Extrude→Areas→Along Lines→Select the area created in step 2→OK→Select the spline→OK.

7. Fiber volume meshing:

Preprocessor→Meshing→Mesh Tool→Size Controls→Lines→Set→Pick the 4 lines forming the cross-sectional area→OK→Number of Element div=1→OK

Select Hex, Mapped→Mesh→Select fiber volumes

8. Overlap operation:

Preprocessor→Modeling→Operate→Booleans→Overlap→Volumes→Pick two volumes

9. Contact pairing:

The contact pairings are created in ANSYS using the Contact manager (Figure 76) which can be found under: Preprocessor→Modeling→Create→Contact Pairs. The contact wizard button (marked in red) in the contact manager is used to create a new contact pair. In the contact wizard page 1 (Figure 76), 'Areas' is selected under the target surface and 'Flexible' is selected under the Target type. 'Pick target' button is clicked to pick a target. The target is usually the concave surface in the contact-pair as per the rule of thumb. In the contact wizard page 2 (Figure 76), 'Areas' is selected under the Contact surface and 'Surface-to-Surface' is selected under the Contact element type. 'Pick contact' button is clicked to pick a contact. The contact is usually the convex surface in the contact-pair as per the rule of thumb.

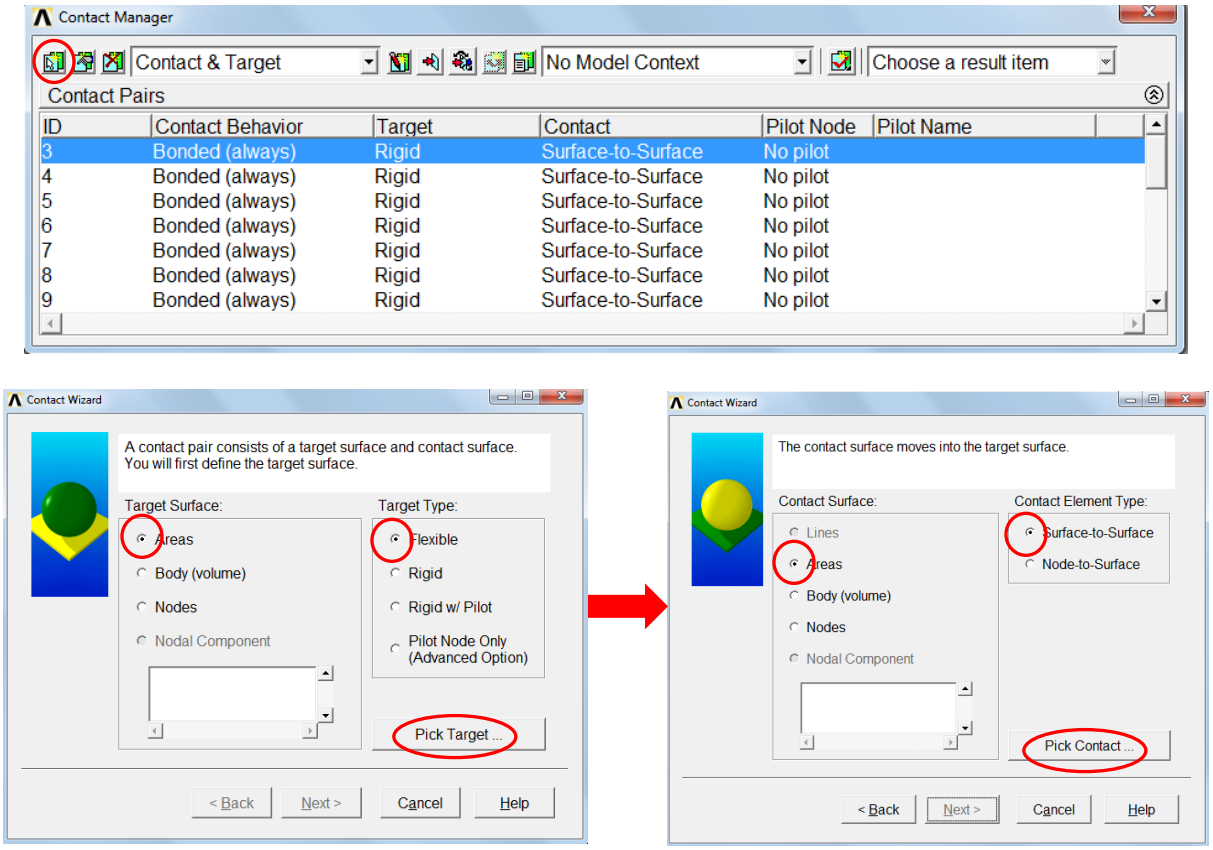

Figure 76: Contact wizard steps for generating contact pairs

In the final page of contact wizard (Figure 77), the Include initial penetration option is checked 'OFF' and under Optional setting→Basic→Behavior of contact surface→Bonded (Always) is selected.

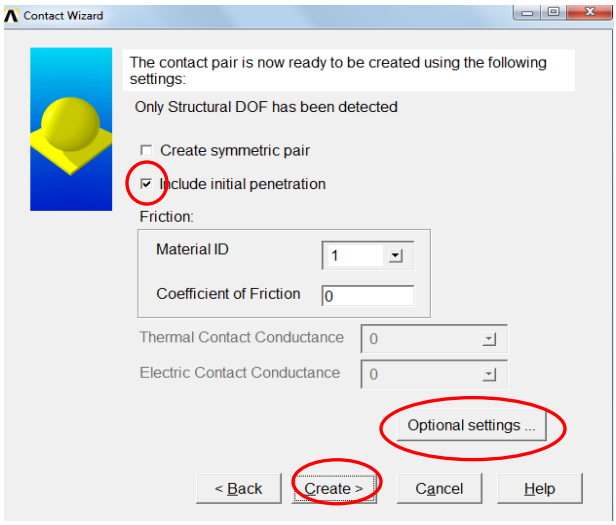

Figure 77: Contact wizard important optional settings

10. Calculation of volume of geometry before/after deformation in ANSYS

Initial volume: Select→Entities→Elements→By Attributes→Material number=3 List→Picked Entities→Query Item=Volume, On Entities→Elements→Pick All

The sum of all element volumes of the particular material type is displayed

Final Volume: General Postprocessing→Element Table→Define Table→Add→Geometry→ Volume→Sum of Each Item→OK

The sum of all deformed element volumes of the particular material type is displayed

Appendix F: ANSYS modeling issues

In our ANSYS modeling, various difficulties/problems were faced and subsequently solved, which are worth mentioning:

1. LV main volume meshing issue:

While trying to mesh the LV main volume, due to its complex and un-friendly geometry, the following two errors were observed: (Figure 78 A, B)

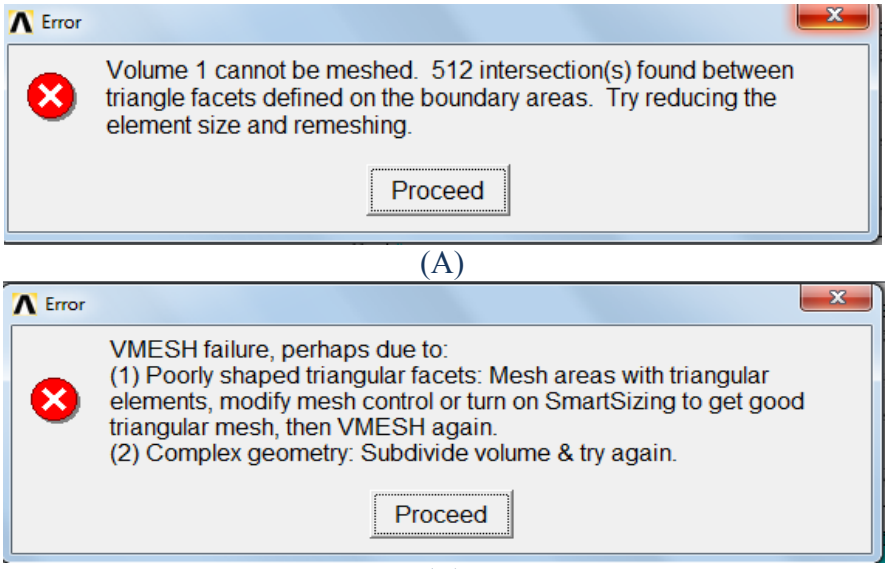

Figure 78: (A, B) ANSYS errors showing difficulty of meshing of LV main volume due to complexities in the geometry

The main volume was subsequently divided into four volumes as shown in Figure 79 (A). However the issue with the four volume geometry was during fiber plotting in ANSYS, more than 4 endocardial (inner) fiber volumes came out (Figure 79 A) of the main volume cutting the main volume at sharp edges (marked in Figure 79 B), and causing mesh difficulties in both the main LV volume and the fiber volumes which came out. The cause of the issue was identified to be the small curvature of the four volumes and a relatively large curvature of the endocardial fiber volumes leading to the fibers coming out of the main volume rather than staying all way in at $1/3^{rd}$ of the thickness from the inner surface.

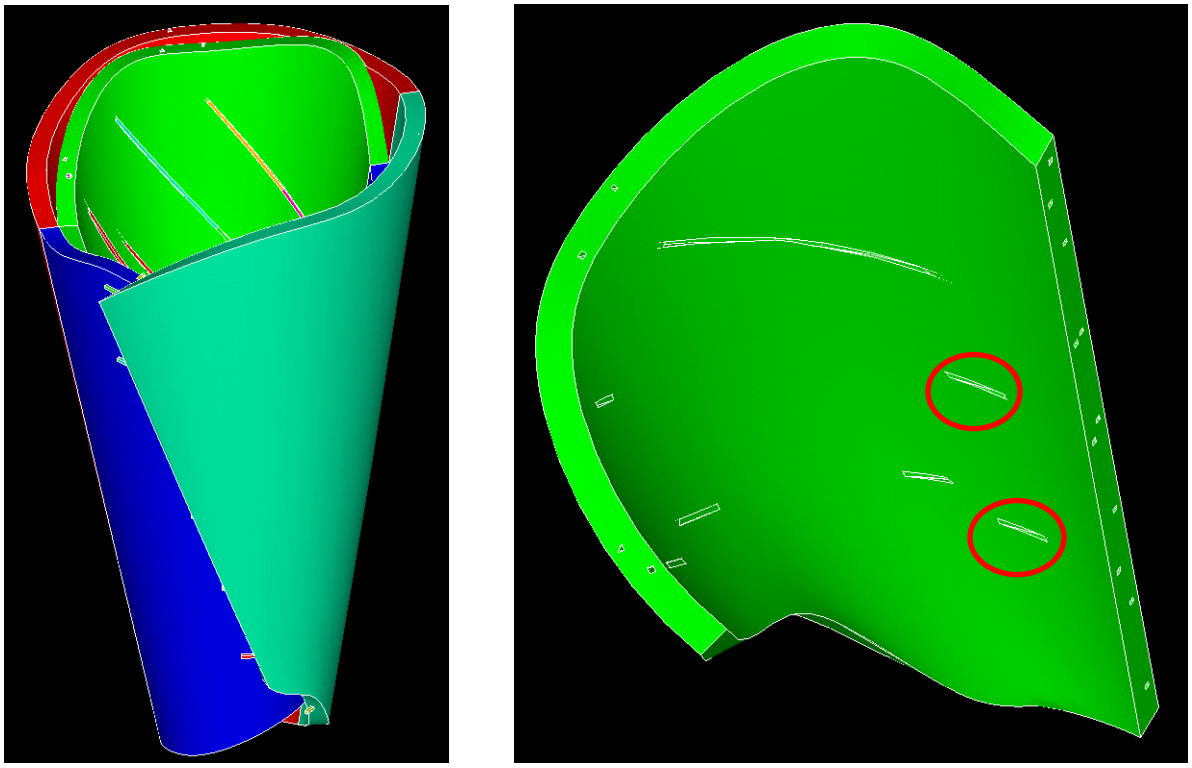

(A) (B)

Figure 79: (A) Main volume subdivided into four volumes. 4 fibers can be seen to come out of the main volume due to curvature issues. (B) Fibers cutting a main volume sub-volume at sharp edges, which may cause mesh difficulties/failure

The issue was solved by dividing the main volume into the maximum possible number of volumes (24 in this case). This subdivided volume meshed well and also none of the endocardial fibers came out of the main volume. In fact all the endocardial fibers were observed to be at 1/3rd thick ness distance from the inner surface throughout.

2. Fiber twisting and meshing issue:

The fiber volumes created using extrude operation couldn't be meshed (Error in figure 80) as it is twisted (encircled in red). To solve this issue, each fiber spline was divided into at least 3 short splines and then the normal area was extruded to obtain 3 volumes (Figure 81).

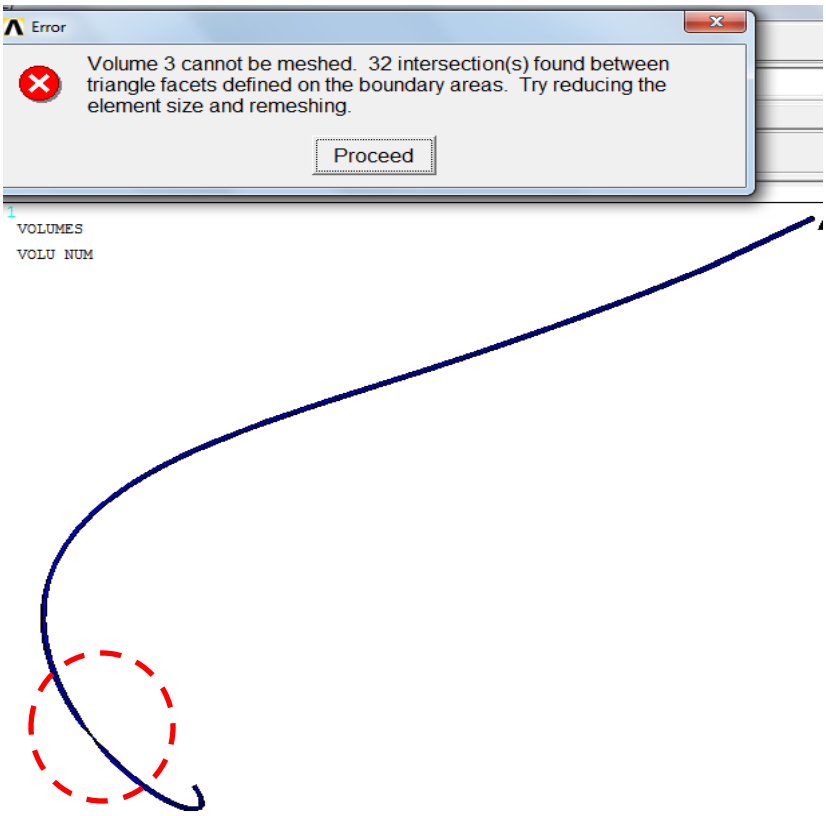

Figure 80: Mesh difficulty in a fiber due to volume twisting (marked in red)

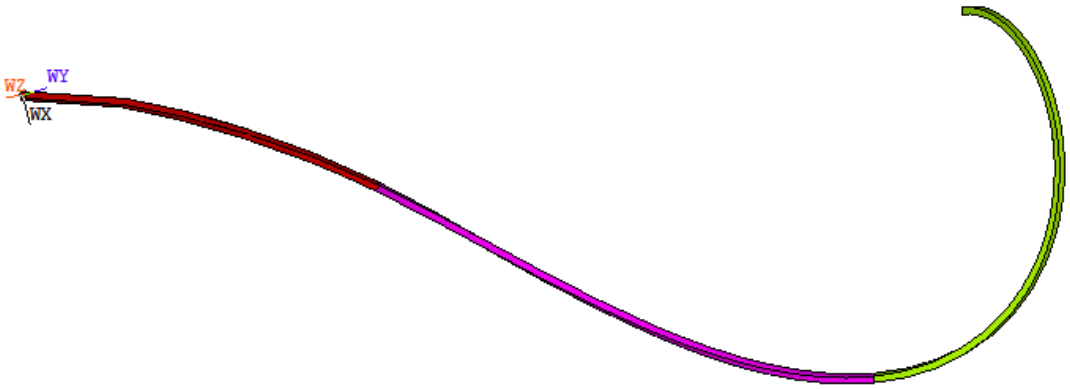

Figure 81: One fiber volume divided into 3 sub-volumes to avoid volume twisting and mesh difficulties

3. Total number of elements generated beyond the permitted limit in ANSYS issue:

In ANSYS, the limitation of the total number of elements is 256,000. As there are a huge number of elements involved in meshing of our entire model with fiber volumes, main volume and an

inner volume, one of the primary considerations while meshing was to reduce the number of elements as much as possible in every step. Thus the meshing of the fibers were controlled using mesh controls. Figure 82 shows the generation of 469 elements in a fiber using regular tet-free meshing.

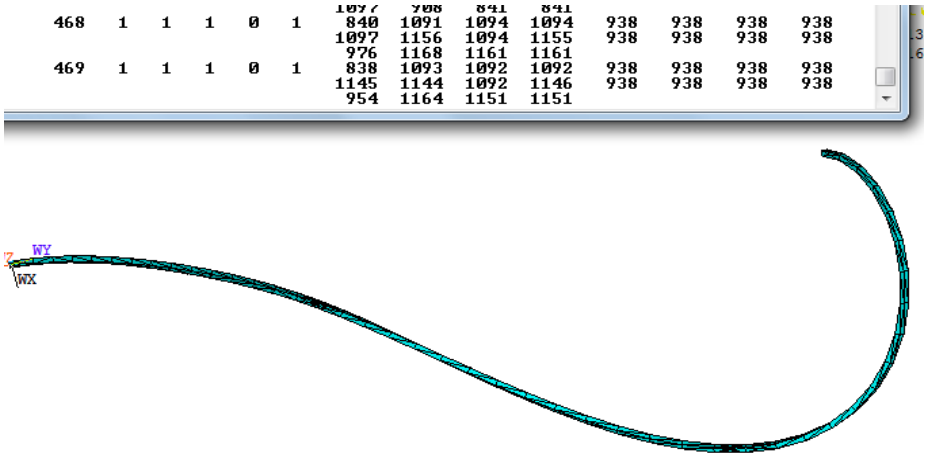

Figure 82: Large number of elements generated due to regular tet-free meshing of a fiber.

To reduce the number of fiber elements drastically, hex-mapped meshing style was used along with appropriate size controls. Figure 83 shows the fiber in Figure 82 re-meshed using Hex-Mapped mesh and size controls, generating only 45 elements.

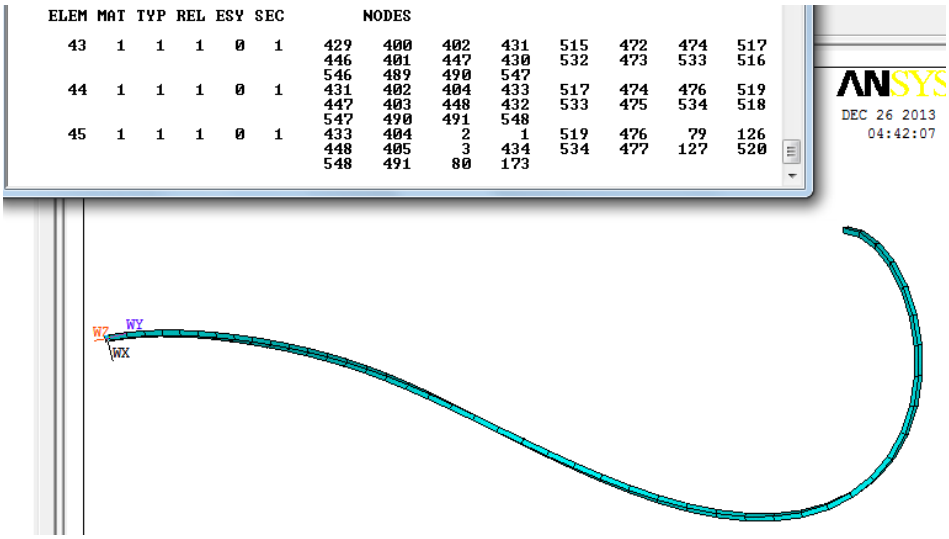

Figure 83: Small number of elements generated due to Hex-mapped meshing (using size controls) of the same fiber in Figure 82.

4. Issue with some fibers coming out of LV main volume:

An issue observed during fiber plotting was that some of the fibers came out through the top and bottom surfaces of the main volume by a bit as shown in Figure 84 (marked in red). This is not desired, as ideally all the fibers should be embedded inside the LV main volume. To take care of this issue, all such fibers were identified and their ends were trimmed off by a bit to have a reasonable amount of gap between the starting/ending fiber points and the top/bottom surfaces of the LV main volume. One corrected fiber end with a reasonable gap is marked in Figure 84 in yellow.

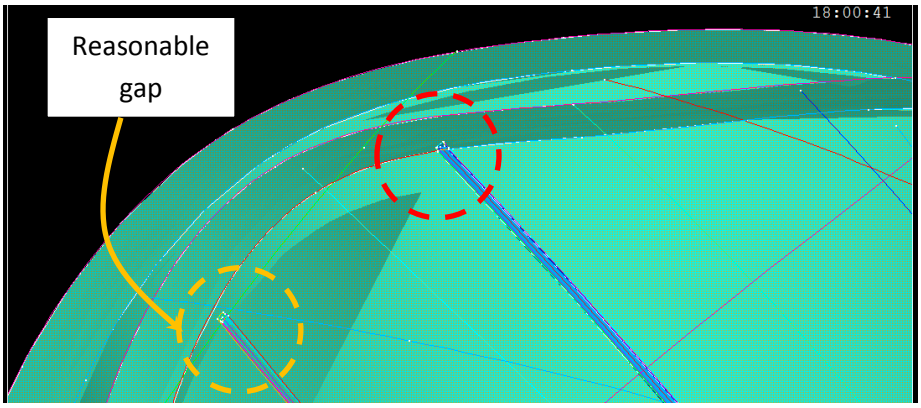

Figure 84: Small gap (marked in red) between a fiber top/bottom and the LV main volume top/bottom surfaces can cause mesh difficulties. A reasonable gap created by trimming of a fiber end is marked in yellow.

Appendix G: LV wall thickening Effect

In 1969, Mitchell et al [41] reported that the LV wall thickness increases from 20% in diastole (filling) to 80% in systole (emptying). Spotnitz et al [42] in 1976 conducted experiments with a dog's heart to validate the LV wall thickness change, which was previously reported by Mitchell et al (Figure 85). During systole, the LV wall was observed to thicken radially outward, shorten along the apex-base direction, and also shorten circumferentially. Also an apical twist was

observed. As a result, the left ventricular wall dimensions were concluded to vary in all directions.

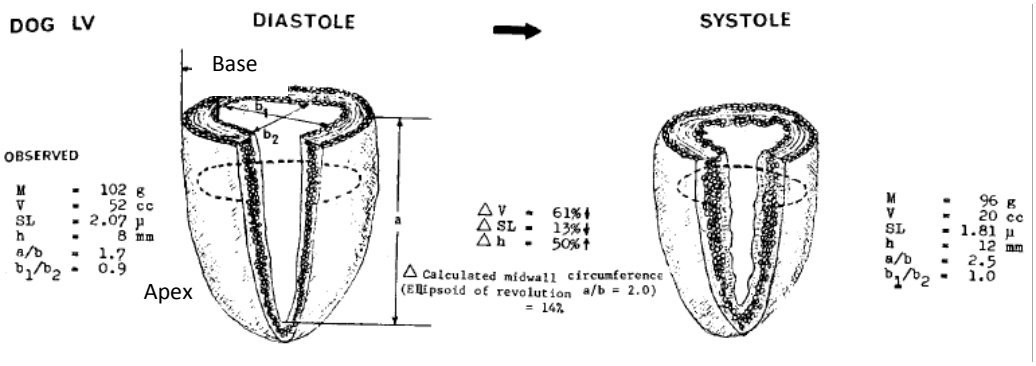

Figure 85: Changes in a dog's LV dimensions, observed during Systole and Diastole phase. Reproduced from [35]

Appendix H: Boundary conditions in the heart

In the heart, the boundary conditions significantly affect the pumping action of the ventricles. The major constrained parts in the heart are namely the base, apex, ventricular valves and the pericardial sac [45]. Figure 86 shows the various boundary conditions adopted in the well-known Auckland heart model [45].

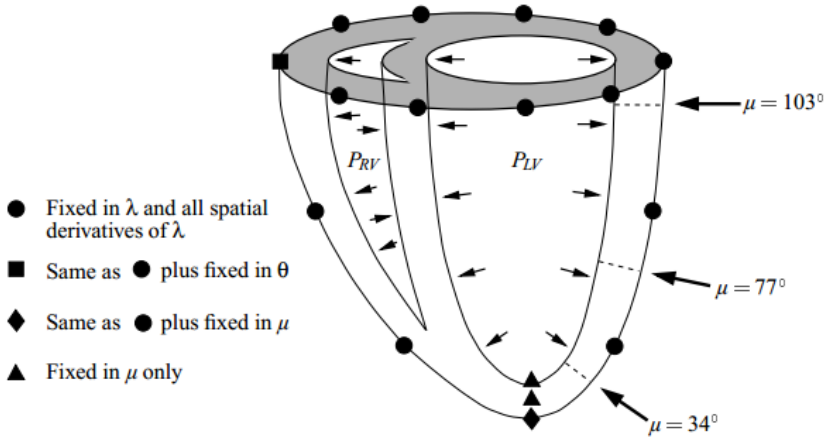

Figure 86: Various boundary conditions adopted in Auckland heart model [45]. 'λ' refers to the radial direction and 'μ' refers to the trans mural direction in the spheroidal coordinate system